

EXPERIMENTAL STUDY ON WIRE MESH SOLAR AIR HEATER

A

Dissertation

Submitted in Partial Fulfillment of the Requirements for the Award of the degree

of

Master of Technology

in

(Thermal Engineering)

Submitted

By

PANKAJ KUMAR

(ROLL NO. 2K18/THE/19)

Under the

Supervision of

Dr. RAJESH KUMAR

&

Dr. ANIL KUMAR



DEPARTMENT OF MECHANICAL ENGINEERING

DELHI TECHNOLOGICAL UNIVERSITY

(formerly Delhi College of Engineering)

Bawana Road, Delhi – 110042

APRIL 2022

DELHI TECHNOLOGICAL UNIVERSITY

(Formerly Delhi College of Engineering)

Bawana Road, Delhi – 110 042

CANDIDATE'S DECLARATION

I, PANKAJ KUMAR, Roll No. 2K18/THE/19 student of M.Tech. (Thermal Engineering), hereby declare that the project Dissertation titled **“EXPERIMENTAL STUDY ON WIRE MESH SOLAR AIR HEATER”** which is submitted by me to the Department of Mechanical Engineering, Delhi Technological University, Delhi in partial fulfillment of the requirement for the award of the degree of Master of Technology is original and not copied from any source without proper citation. This work has not previously formed the basis for the award of any degree, Diploma Associateship, fellowship, or other similar title or recognition.



PANKAJ KUMAR

Roll No. 2K18/THE/19

Place: Delhi

Date: 05/04/2022

DELHI TECHNOLOGICAL UNIVERSITY

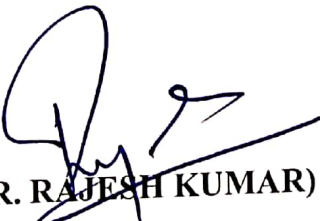
(Formally Delhi College of Engineering)

Bawana Road, Delhi -110042

CERTIFICATE

This is to certify that Project Dissertation entitled “**EXPERIMENTAL STUDY ON WIRE MESH SOLAR AIR HEATER**”, which is submitted by PANKAJ KUMAR, Roll No. 2K18/THE/19 Department of Mechanical Engineering, Delhi Technological University, Delhi in partial fulfillment of the requirement for the award of Degree of Master of Technology is the record of the project work carried out by the student under our supervision. To the best of our knowledge this work has not been submitted in part or full for any Degree or Diploma to this University or elsewhere.

PROJECT GUIDE


(DR. RAJESH KUMAR)
Professor-MED


(DR. ANIL KUMAR)
Associate Professor-MED
Associate Professor
Mechanical, Production & Industrial and
Automobile Engineering Department
Delhi Technological University
(Formerly Delhi College of Engineering)
Shahbad Daulatpur, Bawana Road, Delhi-42

Date: 05/04/2022

Place: New Delhi

ACKNOWLEDGEMENT

I, PANKAJ KUMAR, take this momentous opportunity to express my heartfelt gratitude, ineptness & regards to the vulnerable and highly esteemed main guide, DR. RAJESH KUMAR, Assistant Professor, and co-guide DR. Anil Kumar, Associate Professor, Department of Mechanical Engineering, Delhi Technological University for providing us an opportunity to present our project on “**EXPERIMENTAL STUDY ON WIRE MESH SOLAR AIR HEATER**”. I with full pleasure converge our heartiest thanks to Professor S K Garg, HOD, Department of Mechanical Engineering, Delhi Technological University for their invaluable advice and wholehearted cooperation without which this project would not have seen the light of day. I attribute the heartiest thanks to all the faculty of the Department of Mechanical Engineering and friends for their valuable advice and encouragement.



PANKAJ KUMAR

(2K18/THE/19)

Department of Mechanical Engineering,
Delhi Technological University

ABSTRACT

Using Experimental Research, a parametric study was performed of a Wire mesh solar air heater natural convection SAH. For the analysis, a SAH with a single glass cover is selected as a flat plate solar collector with wire mesh Under the DTU Delhi climate conditions, India. The study aims to find optimum collector efficiency and taking seasonal variations into beam radiation and diffused radiation, seeking input and observing the output variable parameter Impact on collector output of incident radiation magnitude and ambient temperature, all equations, the framework, the governing continuity, momentum and energy equations were considered. SAHs have been used for heating, drying, and similar industrial applications which require heating, drying, and other heated air at temperatures that are low to moderate. SAH (collector)'s performance is a feature of many criteria for design and operation. The heat from convective HT coefficient between the A_{bp} and the air due to one of the main parameters is the collector duct. It is possible to use the air on the right side of the A_{bp} of the SAHs for their thermal output. The TH_{eff} of a SPSAH with wire mesh was examined only experimentally.

A comparison of the effects of solar collector MFRs with and without wire mesh shows a significant increase in TH_{eff} . This experiment deals with the T_{out} °C and performance of the experimental inquiry, of the WMSAH. The experimental test was planned and manufactured to research the effects of WMSAH, by the axial fan in a solar duct flow, on the wire mesh solar air heater compared to the traditional SAH on a FPC's A_{bp} , under the effect on the T_{out} °C of the MFR of air and SI, results, are analyzed.

The findings of experimental research on the T_{thp} of a WMSAH are provided in this experiment. In direction to maximize the surface of heat exchange, the T_{out} °C, and TH_{eff} , a black wire mesh for an A_{bp} must be designed in particular. Tables 7.1a show that for the SAH without wire mesh and a black A_{bp} , increases in MFR affect the temperature of the wire mesh and the temperature of an A_{bp} by 5 to 6 °C.

By rates of 5.3 percent and 6.13 percent, the TH_{eff} of the type with WMSAH is shown to be higher than the FPC. We can improve this SI by adding wire mesh above the A_{bp} for moving the heat energy in between the A_{bp} and the wire mesh and the heat energy on an A_{bp} for transportation of fluid with the MFR of 0.012 and 0.016 kg s⁻¹; see Tables 7.3a and 7.3b, and a lesser SI by rates 162 and 187W m², respectively; we can recover this loose SI by adding wire mesh above the A_{bp} for moving the heat energy in between 27.92 percent and 42.83 percent, respectively, were the maximum TH_{eff} figures measured.

CONTENTS

Candidate Declaration	2
Certificate	3
Acknowledgement	4
Abstract	5
Contents	6
List of Figures	7
List of Tables	8
Chapter 1: Introduction	13-21
1.1.1: Requires Of Global Energy	10
1.1.2: Non-Conventional Energy Scenario	11
1.1.3: Global Consumption of Solar Energy	13
1.1.4: The Re Capital Overview	15
1.1.5: The Energy Forecast	15
1.1.6: Solar Energy's Limits	15
Chapter 2: Literature reviews	22-32
2.1: Objective of the present study	25
2.2: Literature Reviews	32
Chapter 3: Methodology	33-34
3.1.1: Thermal Analysis of Flat Plate Collector	33
3.1.1: Solar Radiation of Inclined Plane Surface	34
Chapter 4: Fabrication of Solar Wire Mesh Air Collector at Green Lab Delhi	35-42
Chapter 5: simulation of solar wire mesh air heater	43-45
Chapter 6: Results & discussion	46-49
Chapter 7: Conclusions	50
References	59

LIST OF FIGURES

Figure 1.1: World energy outlook 2005	13
Figure 1.2: Shares of renewable resources in global electricity capacity	15
Figure 1.3: Spectral irradiance curve for direct sunlight	15
Figure 1.4: Global energy consumption	16
Figure 1.5: The wbu(2003) global energy mix 2050 and 2100	19
Figure 4.1.1: Main body of solar wire mesh air collector	35
Figure 4.1.2: Installing the thermocouple on absorber plate	36
Figure 4.1.3: Installing of the thermocouple on wire mesh	36
Figure 4.1.4: Fan assembly installation with duct	36
Figure 4.1.5: Fan back view	37
Figure 4.1.6: Fan dimension	37
Figure 4.1.7: Installation of fan at the inlet of wire mesh collector	39
Figure 4.1.8: fixing of glass on wire mesh air heater	40
Figure 4.2.1: Hygrometer	41
Figure 4.2.2: Temperature indicator	41
Figure 4.2.3: Solar power meter	42
Figure 4.2.4: Testo 416 anemometer for measuring of air velocity	42
Figure 5.1.1.a: Isometric view	43
Figure 5.1.1.b: Top view	43
Figure 5.1.1.c: Bottom view	44
Figure 5.1.1.d: Front view	44
Figure 5.1.1.e: Back view	45
Figure 5.1.1.f: Left view	45
Figure 5.1.1.g: Right view	45
Figure 6.1a: Avg. temp for flat plate and wire mesh type collector ($m=0.014\text{kg s}^{-1}$ 0.014 kg s^{-1} , for solar collector thickness for 3mm with tilt angle $\beta=45^\circ$)	47
Figure 6.1b: Avg. temp. for flat plate and wire mesh type collector ($m=0.014\text{kg s}^{-1}$ 0.014 kg s^{-1} , for solar collector thickness for 3mm with tilt angle $\beta=45^\circ$)	48
Figure 6.1b: Wire mesh type collector corresponding to $m=0.014\text{kgs}^{-1}$, for solar collector from 0.388m to 1.552m	49
Figure 6.3a: Solar intensity and thermal efficiency versus time of the day for flat plate collector	

corresponding to the $m=0.014\text{kgs}^{-1}$, according to the time of the day, between 09:00 and 16:00, for solar collector with tilt angle $\beta=45^\circ$ 50

Figure 6.3b: Solar intensity and thermal efficiency versus time of the day for wire mesh type collector corresponding to the $m=0.014\text{kgs}^{-1}$, according to the time of the day, between 09:00 and 16:00, for solar collector with tilt angle $\beta=45^\circ$ 51

Figure 6.4a: Temperature versus different standard local time during days at $m=0.014\text{kgs}^{-1}$ with tilt angle $\beta=45^\circ$ corresponding to outlet, inlet and ambient temperature of flat type solar collector 52

Figure 6.4b: Temperature versus different standard local time during days at $m=0.014\text{kgs}^{-1}$ with tilt angle $\beta=45^\circ$ corresponding to outlet, inlet, and ambient temperature of wire mesh type solar collector 53

Figure 6.5a: Comparison between efficiency of flat plate and Wire mesh type collector 54

LIST OF TABLES

Table 1.1: Fuel shares in world total primary energy supply	12
Table 1.2: Re-technologies ability and status	15
Table 1.3: Solar electric energy from Earth's high-insolation areas	17
Table 7.1a: Table Temperature variation of FPC and WMSAH along thickness(Y)m	47
Table 7.2a: Flat plate solar air heater	48
Table 7.2b: Wire mesh solar air heater	49
Table 7.3a: Flat plate collector SI and efficiency	50
Table 7.3b: Wire mesh type collector SI and efficiency	51
Table 7.4a: Flat plate collector inlet and outlet temperatures	52
Table 7.4b: Wire mesh type collector inlet and outlet temperatures	53
Table 7.5a: Comparison between flat plate and wire mesh type collector efficiency	54

NOMENCLATURE

DTRM - Discrete transfer radiation Model

SAH - Solar air heater

NPSAH – non-porous solar air heater

N_u – Nusselt no

F_f – Friction factor

CFD- Computational fluid dynamics

A_{bp} – Absorption plate

TH_{eff} – Thermal efficiency

CF – counter flow

SPSAH – single-pass solar air heater

dPSAH - double pass solar air heater

B_f – Baffles

Logf - longitudinal fins

nVrib – multiple V-shaped ribs

R_e - Reynolds no

P_d – Pressure drop

V_{rib} – V down rib

SWM – Steel wire mesh

WM – wire mesh

SPSS-IBM - Statistical kit for social sciences software of IBM

MFR – Mass flow rate(kg/s)

WML – wire mesh layer

F_c – forced convection

C_{sa} – surface area of collector

N_c – natural convection

T_{thp} – Thermal performance

AV – average

DPFIPSAH – Double pass finned plate solar air heater

DPVCPSAH – double pass V corrugated plate solar air heater

WMSAH- Wire mesh solar air heater

FPC- flat plate collector

SI-solar intensity w/m^2

T_{ab} – Temperature of an absorber plate in degrees Celsius

T_{bp} - Temperature of wire mesh in degrees Celsius

T_{pl} – Temperature of air in between of absorber plate and wire mesh

T_{ep} – Temperature of the glass of wire mesh solar air heater

T_{in} – Temperature of inlet air of solar air heater in degrees Celsius

T_{out} – Temperature of outlet air of solar air heater in degrees Celsius

T_a – Temperature of ambient air in degrees Celsius

A^0 – Inclination angle of collector from the horizontal surface in degree

α - Absorber plate's absorption coefficient

τ - Glass transmittance coefficient

α_g - Glass absorption coefficient

T_{HR} - thermal resistant

RE- Renewable energy

T_{av} – Average temperature in 0C

1.1.1 Requires of global energy

Much of the world's energy demand is met by fossil fuels, but the massive extraction of fossil fuels is causing global warming and water cycle acidification to pose a real threat to the environment. The rapidly growing demand for energy, the decreased supply of conventional sources of energy, and the contamination of the atmosphere have driven scientists to look for alternative sources of energy. Among those energy resources, sun and wind are practically limitless and available at no cost in abundant quantities and all over the world.

Global energy demand has risen dramatically in the last half-century. Relatively "cheap" fossil fuels stimulated the prior rise. The use of energy continues in all countries. Rising, additional factors add to the image for the next 50 years complicated. China's and India's contain these additional complicating variables. Rapid rise in the usage of electricity as it accounts for around one-third of the population of the planet, the projected oil loss supplies shortly. The future and the effect of human actions on climate change around the world. On the positive side: Sustainable energy technology for air current power, biological fuels, solar power. (Figure 1.1).

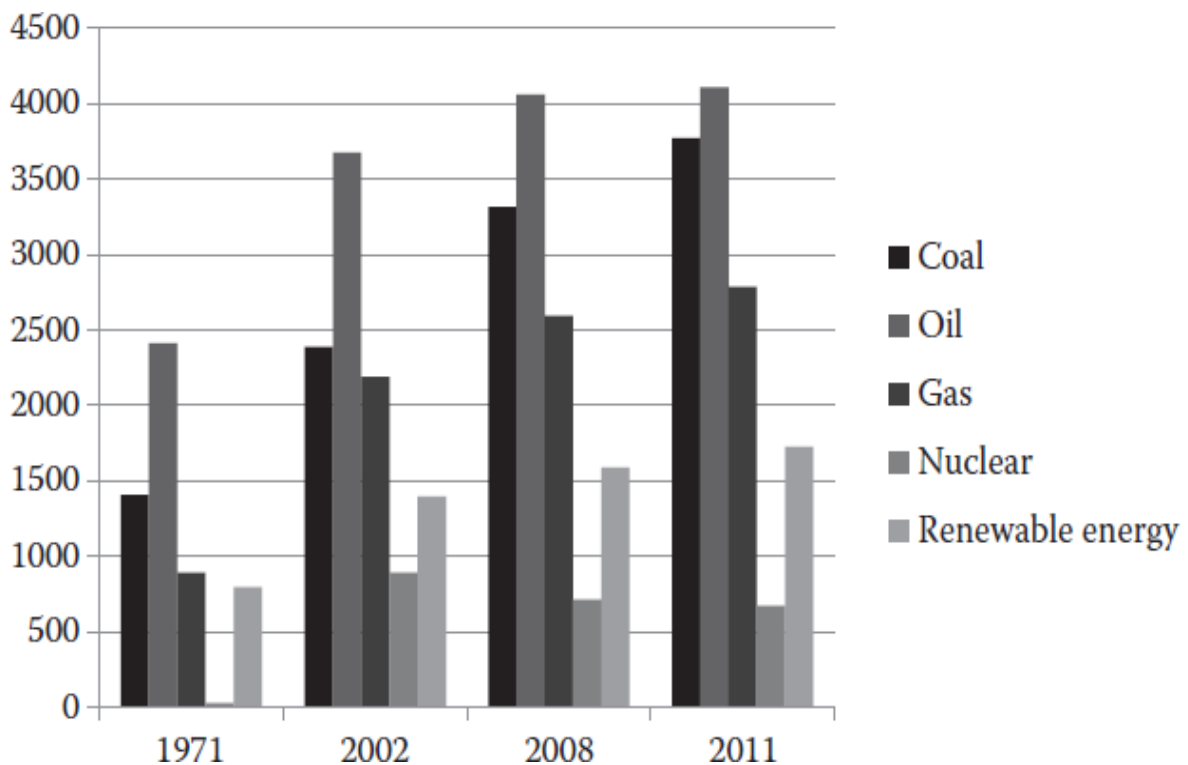


Figure 1.1 World Energy Demand

The need for world energy has risen to reflect 12,271 MTOE of energy. An annual average rise

of approximately 3%. The fast-growing energy demand is a 50 % rise in the annual average. The Asia Pacific, China in particular. Because the used electricity per capita in The many populated States is quite limited, The nation (India) is still very small. At this extremely high pace, the usage of power will keep rising. The real yearly power average boost fell, Due to the extreme growth in the United States and Europe, where the consumption indicates that RE sources will account for as much as 50% of global energy usage in 2050, with the vast majority coming from solar and wind energy.

1.1.2 Non-condensational energy scenario-

Solar power accounted for 13.3% of the world's estimates, according to the data in Table 1.1. 2011 gross primary energy supply. Nonetheless, roughly 75% of the supply of RE is from biomass and is primarily converted by conventional open combustion in developing countries, which is very inefficient because biomass services currently only supply roughly their inefficient usage, 20% of what they could do if they were converted into new, more effective, accessible technology. In 2011, the overall proportion of all renewables for the production of electricity was 20.4%, of which the vast majority (78%) came from hydro-powered energy. Although the global capacity of renewable energy accounted for just 1.34% of complete potential for power, it expanded by approximately 50% annual average.

Table 1.1: The share of fuel in the world's total primary energy supply

Fuel share in the world's total primary energy supply	
SOURCE	SHARE
OIL	31.4%
NATURAL GAS	21.3%
COAL	28.9%
NUCLEAR	5.2%
RENEWABLE	13.2%
Total	20%

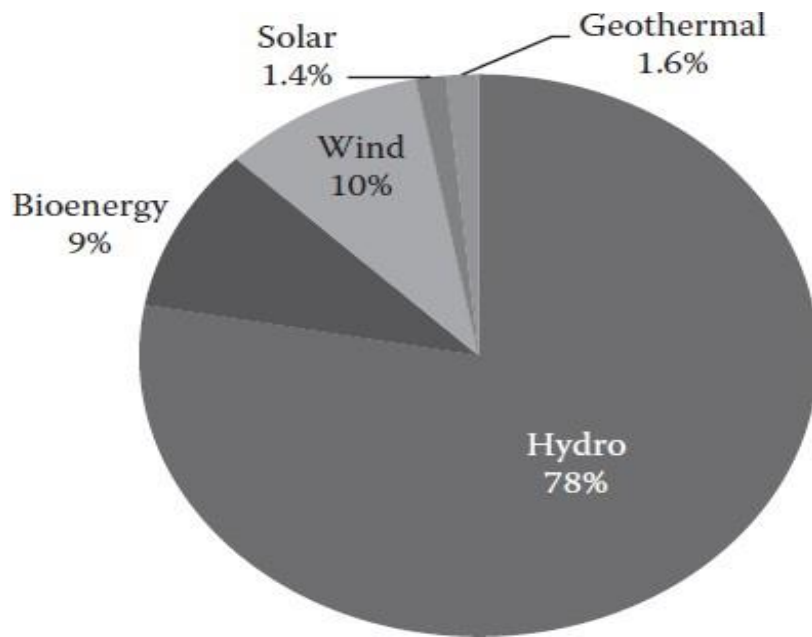


Figure 1.2: Outlook of Global Energy

1.1.3 Global consumption of solar energy

The incident of SI on a surface unit is referred to as radiance time. The average natural extraterrestrial irradiance to the solar beam is roughly 1.36 kW/m^2 in the ecosystem of the earth. Using thermal and photovoltaic conversion devices, solar energy can be a significant energy source and can be harnessed. On a bright sunny day, at noon, the mean solar radiation received on the surface of the earth, natural to it, is approximately 1 kW/m^2 , at sea level.

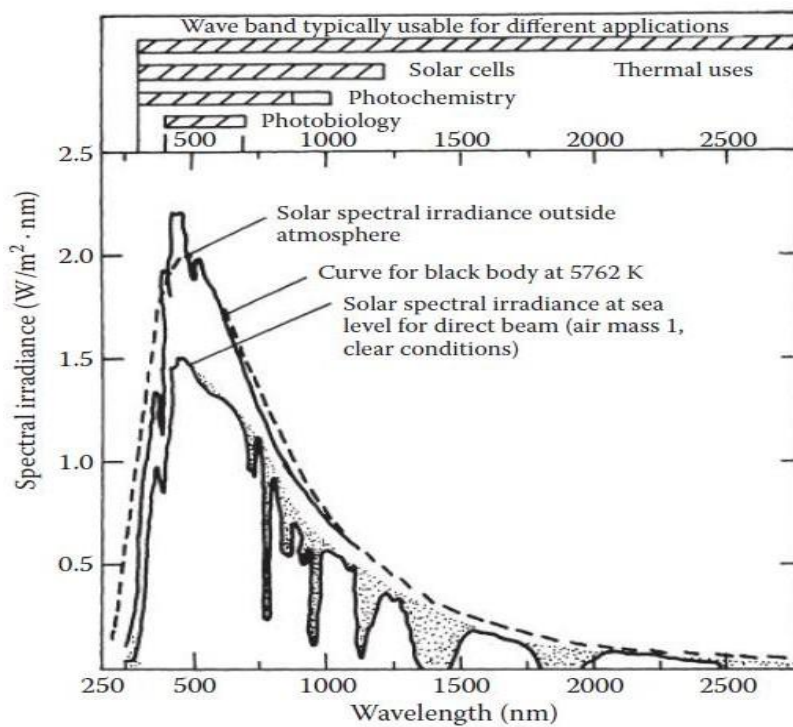


Figure 1.3: solar spectral irradiance curve for direct sunlight.

The earth continually intercepts 178 billion mW of solar electricity, which is about 10,000 times the world's production. But it has not been able to grow on a wide scale so far. According to one calculation, if all the world's buildings are protected by solar PV panels, they would meet the world's electrical power requirements. It is considered that solar PV energy is a costly source of electricity. However, rates are slowly declining. In the last 20 years, the cost of the SPV system has fallen from USD 10 per W to USD 3 per W. The use of solar energy is increasing strongly across the world, partially due to the rapidly decreasing cost of producing solar panels.

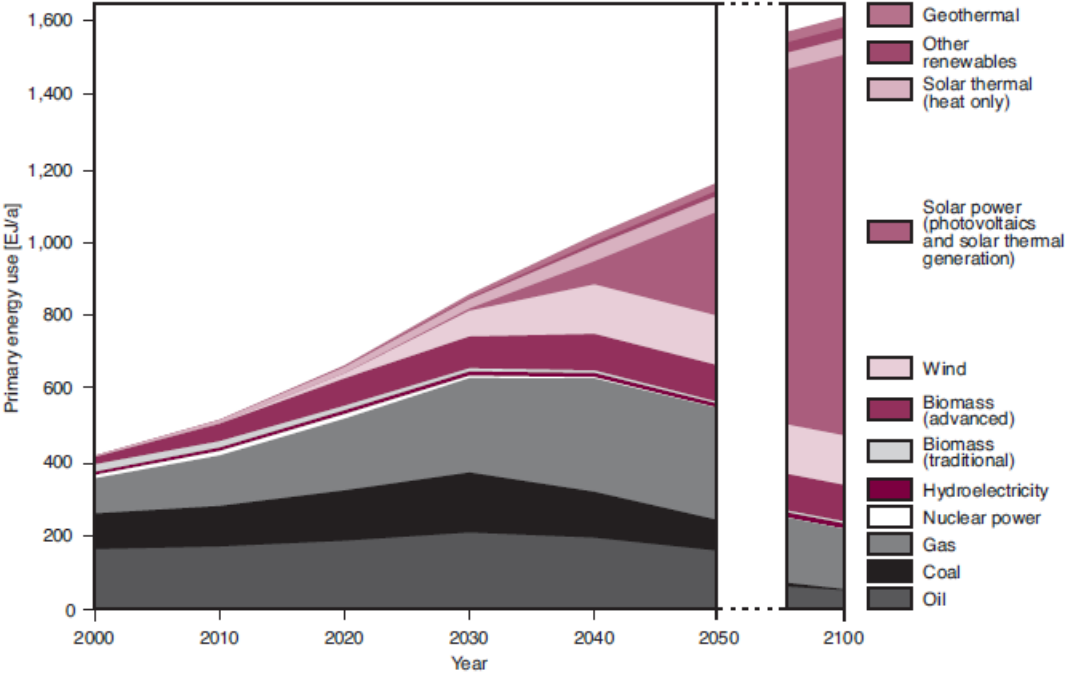


Figure 1.4: Global energy consumption

Normally, its value is per nanometer of bandwidth, calculated in watts per square meter. The extraterrestrial radiance of the spectrum. The sum of sunlight that continuously strikes the atmosphere of the earth is 1.75 TW by 105. Provided a transmission through the atmosphere of 60 % Cloud coverage, $1.05 \cdot 10^5$ TW continually reaches the surface of the earth. The efficiency of multijunction solar cells under the concentrated sun has surpassed 40% and solar thermal systems have 40 per cent-60 % TH_{eff} . The cost of solar PV panels has fallen from around \$30 / W to \$30 / W. In the last three decades, \$0.50/W roughly. There has been a revival of interest in this field in the last 10 years, however, and many solar-based thermal power plants around the world are undergoing Building Design. The largest CSP plant with a 400 MW capacity was installed. In 2014 in Nevada cost of plants' electricity (it can go down in a range of 12 to 16 US cents / kWh) to 5 US cents / kWh with a mass market.

1.1.4 The RE Capital Overview

Table 1.2: Renewable energy-oriented capital overview table

Technology	Annual potential	Operating capacity 2005	Investment cost US\$ per kW	Current energy cost	Potential future energy cost
Biomass energy Electricity Heat Ethanol Biodiesel	8-13TW	44GW _e 225GW _{th} 36 billion lit. 3.5 billion lit.	500-6000/Kw 170-1000/Kw 170-350/Kw 500-1000/Kw	3-12\$/kwh 1-6\$/kwh 25-75\$/lit. 25-85\$/lit.	3-5\$/kwh 1-5\$/kwh 6-10\$/Gl 10-15\$/Gl
Wind power	55TW theor 2TW practical	59GW	850-1700	4-8\$/kwh	3-8\$/kwh
Solar energy Photovoltaics Thermal power Heat Geothermal Electricity Heat	>100TW 600,000EJ Useful resource 5000EJ for 50years	5.6GW 0.4GW	5000-10000 2500-6000 300-1700	25-160\$/kwh 12-34\$/kwh 2-25\$/kwh	5-25\$/kwh h 4-20\$/kwh h 2-10\$/kwh h

				2- 10\$/kwh 0.5- 5\$/kwh	1- 8\$/kwh 0.5- 5\$/kwh
Ocean energy					
Tidal	2.5TW	0.3GW	1700-2500	8-	8-
wave	2.0TW		2000-5000	15\$/kwh	15\$/kw
otec	228TW		8000-20000	10- 30\$/kwh 15- 40\$/kwh	h 5- 10\$/kw h 7- 20\$/kw h
Hydro electricity	1.63THEO- RYTICAL 0.92TW ECONOMICAL				
large		690GW	1000-3500	2-	2-
small		25GW	700-8000	10\$/kwh 2- 12\$/kwh	10\$/kw h 2- 10\$/kw h

As in the matter of new emerging technologies, RE technology is expected to have research and development, company experience, and manufacturing processes, sustainable costs can be achieved. For any of the combined output for experience demonstrates industry-wide cost savings in the range of 10 % to 20 % from wind power, solar plants, ethanol, and gas turbines. In CSP and other renewable technologies, similar declines can be expected. Market maturity has already been

reached by wind energy technologies, solar energy systems are well on the way. It does have an installed capacity of 40 GW or so.

1.1.5 Energy Forecast

Restricted oil, gas, and nuclear power. It seems obvious that resources and significant global concerns with regards to carbon components, renewable energy resources would not only require solar power, wind power, and agriculture however waste can already take its place and provide a solution for the future. For renewable green technology. On the potential energy mix, there are several conflicting viewpoints. However, we believe with the WBGU, which forecasts that as much as 50 % of the global electricity production in 2050 will have to come from solar power. it will take a worldwide dedication and an unparalleled global initiative to reach the degree of RE usage by 2050.

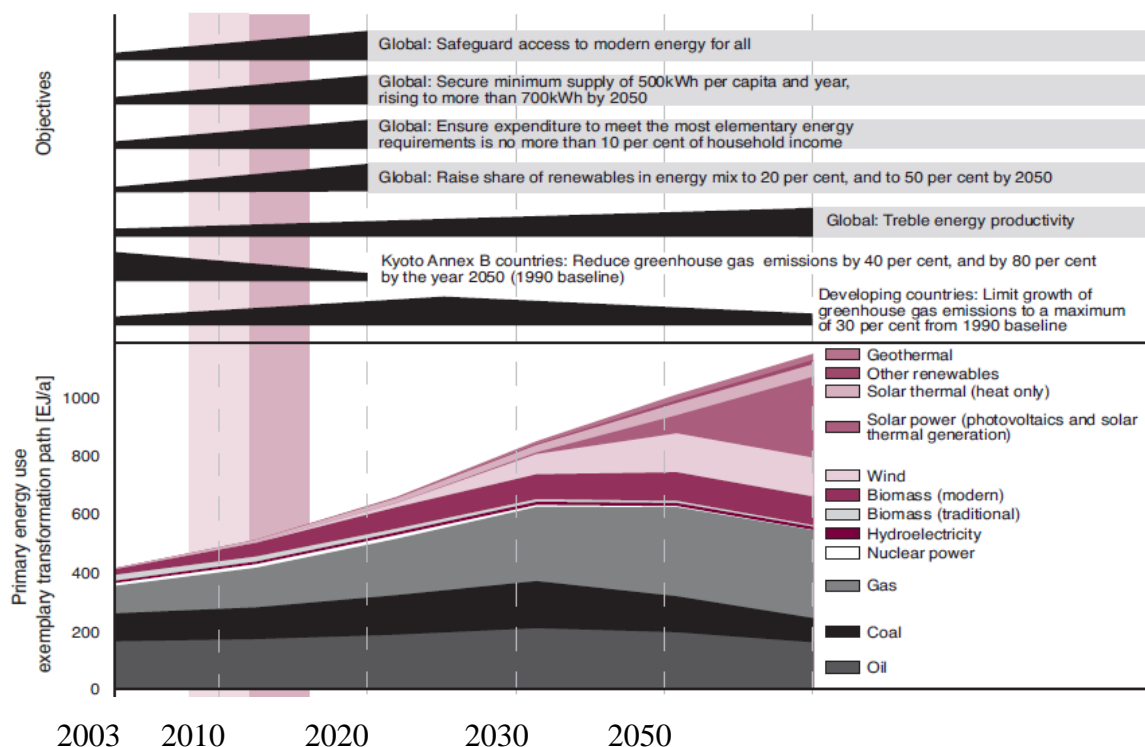


Figure 1.5: The WBGU Global Energy Mix for 2050 and 2100.

1.1.6 Solar Energy's Limits

The first challenge found in the engineering design of machinery for the low flux density is the use of solar energy, which makes high flux densities possible. Solar energy storage surfaces for utilization on a worldwide basis, at higher surfaces, the extra costly the energy distributed becomes. When it's the Sun 10 m² of the surface could potentially provide solar power at a 69.99% collection effectiveness and 29.99% utilization for converting at an average of nearly 2kW directly

overhead on a cloudless day. The total solar energy that reaches the earth, therefore, consists of two main parts: the energy in the direct beam and the diffuse energy from the sky. Many factors minimize this amount in practice. The addition of the cloud cover affects direct energy, and location of the sun, and on bright days, it is certainly the greatest. Any solar radiation that falls on clouds is scattered by diffusion, but not all radiation is absorbed by clouds.

The function of the cloud is predominantly to boost the amount of diffuse energy reaching the surface in the summertime with large and split clouds, the solar energy, and diffuse radiance can be as high as 400 W/m². Dark clouds cause a smaller amount of solar energy to move instead of weak clouds and distribute back in, space too much of the amount of energy proportionally. A second environmental, practical constraint, which isn't evident from the point of vision of macroscopic energy. It is just that the majority descends in renewable energy in inaccessible areas and to be important to develop nations, several other forms of distribution would therefore be required.

Around the latitudes of 25 °N to 25 °S of the equator in continental desert regions, via a horizontal, the total power available is maximum and falls towards both the poles and the equator. While in the area of a Red Sea, the highest annual average radiance is 300 W/m². Clouds in equatorial regions greatly decrease the mean global irradiance.

The direct and diffuse surface irradiance average varies from summer to winter. The season, in equatorial regions, remains relatively constant. Typical Qualities of The mean annual horizontal surface irradiance is as follows: In Aust, roughly 200 W/m²; in the U.S. and Canada, 185 W/m²; in the UK, 105 W/m² displays the overall potential of solar power for the world's solar energy-rich areas. It is essential to note all of these places of the globe, like Egypt, central Asia, and parts of Western America. Africa and India are deserts that are unavailable for cultivation.

Table 1.3: Total solar to electrical energy conversion in high insolation area

Desert	Nominal areas(km ²)	Nominal annual thermal energy flux(GWh/km ²)	%age of area assumed useable	Electric energy extracted at 25% efficiency(GWh/year)
North Africa	7,77,0000	2300	15	670,000,000
Arabian peninsular	1,300,000	2500	30	244,000,000
Western and central Australia	1,550,000	2000	25	194,000,000
Kalahari	518,000	2000	50	129,000,000
Thar (northwest India)	259,000	2000	50	65,000,000

Mojave, California	southern	35,000	2200	20	3,900,000
Vizcaino, California (Mexico)	Baja,	15,500	2200	25	
Total average		11,447,500	2190	31	1,308,000,000

It should be acknowledged, at the same time, that these are also regions with slight to no liquid, pointing to some necessity for evolving options for solar air refrigeration thermoelectric Power. While solar energy distribution is globally distributed, favoring the world's developed parts, It's essential to remember to these countries, particularly Europe, that countries have contributed to the introduction of over the last decade, solar power. Its intermittency is the third disadvantage of solar energy as a large-scale power and heat source our planet's revolution on its axes and the natural seasonal period are due to the tilt of the spin-orbit with the elliptical orbit and the earth's movement across the sun, solar energy has a regular daily cycle and is often inaccessible during times the winter weather conditions. Is therefore obvious that this kind of conservation is indicated by these weather patterns solar radiation variations, worsened by weather fluctuations. Or a supplement for gasoline.

2.1: Objective of the present study

A systematic aim of the literature review is to collect background information about the topics to be considered in the current research. The article provides a brief overview of the strategies implemented to boost or improve the conduction of energy. These are some of the different areas of techniques considered to improve the conduction of energy from F_c . To get a higher HT coefficient, the current will be turbulent nearest to that seen on the HT surface. However, the energy needed to produce such turbulence is generated by the blower or fan. The excessive turbulence results in excessive power demand for duct airflow. To increase its efficiency, it is therefore important to minimize such power loss.

2.2: Literature Reviews

Gagandeep and Sandeep [1] did research that reflects on the different configuration criteria taken into consideration when constructing the experimental set-up and the results of these criteria. Two different methods of convection were tested, Convective mode or natural mode to ponder the coefficient of HT correlated by a respective event the output of the solar air collector. To decrease Glass is used to allow air to circulate through several passes through shading losses. To forecast the air temperature pattern with the term radiation model and design Turbulent, a CFD simulation is used. on atmospheric pressure, the setup works. When comparing experimentally with natural convection, the modeling provides good results. Concerning all convection modes, the temperature properties of the air are shown. The total of passes was considered to improve the air duration of the dwelling since the transition heat to midair enhances the loss of pressure, For glass partitions, the shading losses are offset. Around 12 noon to 2 pmon a sunny day, optimum efficiencies are reached.

Alemu Tiruneh et al. [2] did CFD research which was used to perform a simulation investigation on the natural convection “SAH”. For study under the environmental conditions of Addis Ababa, Ethiopia, a “SAH” with a single glass shield solar collector with an air gap is chosen. The goal of the analysis is to find optimum angles of inclination considering the natural fluctuations, find optimum air gap width, and describe the effect on the collector performance of the incident radiation magnitude and ambient temperature. The governing continuity, energy, and laws of energy were regarded now multiple proportions intended for modeling systems. By

adjusting the angle of inclination, it was noticed that for November, the optimum angle of inclination that provides maximal energy gain with better mass flow rate and temperature increase was 45°, while for May it was 15°. The two-pitch angles reflect the two extreme seasons of the year. A collector with 50 mm channel depth was also found to achieve better output velocity and temperature and maximum energy gain, but comparable to 60 mm and 70 mm depth for a 2 m long collector. The performance of the simulation is comparable to the experimental findings published in the literature, which are already accessible.

Chabane et al. [3] experimentally calculated the TH_{eff} of a SPSAH through 5 attached fins. To improve the sharing of Heat and make transverse fins reduced as its A_{bp} is being used for fluid flow in the uniform channel. The impact of the MFR of airflow at the T_{out} °C, HT in the “SHA” depth, or thermodynamic effectiveness have been calculated. In these two airflow velocities for 0.0123 and 0.0165 kg s⁻¹, Tests have been performed. For various airspeeds with and without fins, through comparison, the highest performance values achieved be situated at 40.023 %, 51.505 % also 34.923 %, and 43.943 %, correspondingly. A study of the effects with and without fins of T_{thp} mass flow velocities shows a substantial improvement in TH_{eff} .

Aboghrara et al. [4] study outline the SAH's experimental analysis of T_{out} °C and TH_{eff} . The experimental test was planned and produced to research the influence of jet intrusion on the robust absorber layer through circular jets in the SAH duct flow besides related to traditional SAH proceeding with the A_{bp} of a flat plate. Air and SI radiation are studied under the control of the MFR the degree of temperature also the quality of Outlet air from its outlet. Findings show that impingement of the jet of fluid on the uneven platform is a good thermal enhancing absorption feature. The previous research suggests that the thermal conductivity of SAH is significantly influenced by the mass flow rate. And almost 14 % better than the smooth duct is found in the context of the thermal characteristics of the planned design duct. An average 750 (W/m²) solar radiation, 309.5K atmospheric high temperature, and also approx. 0.02 (kg/s) the rate of mass flow. If the amount of the MFR has increased and the TH_{eff} is improving.

Karwa and Sharma [5] provide a comprehensive mathematical model of a once-through solar water heater for efficiency analysis. The model is validated against the effects of experiments. It was used for a variety of architecture, ambient and operating parameters, and heat transfer enhancement on thermal efficiency and pressure drop to research the solar water heater output. Depending on the flow rate, the selective coating ($\epsilon = 0.1$) collector has thermal efficiency advantage of 9-16%. Collector of 2 mm thick, brazed, or 0.5 mm thick fins Laser or ultrasonic welded thick fins has the same performance. Usage of heat transfer enhancement products, such as a twisted film, for three times heat transfer enhancement, will increase the collector's thermal efficiency by 5.3-6.2%. In the form of concept graphs, the outcomes of the analysis are described

along with the effects of differences in different parameters.

Kumar and Chinnapandian [6] The design and development of a flat plate solar air collector was studied in both steady and transient convection, and it was found that the efficiency of the collector in natural convection provided high efficiency compared to the efficiency of the collector in F_c . However, the thermal loss in forced convection is significantly lower than in

natural convection. Moreover, the shows that the average air velocity was about 25% higher in F_c than the natural convection that is important in solar dryers. The collector efficiency of natural convection is 18.6 trillion times greater than that of induced convection collector efficiency at mid-time.

Saxena et al. [7] examined the design and efficiency of a long-term heat storage SAH. The primary goal of its objective is to increase the HT coefficient and increase the efficiency of simple SAH. He introduced an absorbing medium inside the SAH, viz. granular carbon. Measurement of the SAH's thermal efficiency was achieved via performing it on both Force and normal convection on four separate arrangements of parts or components. To give for air heating and drying warm air, he designed besides manufactured two SAH (S^1) and SAH (S^2) of identical basic proportions. The maximum efficiencies for 's1' were stated to be 16.16%, 19.02%, 17.04%, and 18.16% on normal convection for 4 distinct systems arrangements, though the overall efficiencies for SAH(S^2) were 17.79%, 20.77%, 18.27%, and 18.95% on similar arrangements of natural convection parts.

Singh et al.[8] investigated the friction factor also HT correlations of SAH by distinct V-down spokes as per on the absorber layer, the simulated unevenness He examined the rectangular duct heated the one large wall and artificial roughness provided as V-down ribs subjected to consistent heat flux with Reynolds no shifted as of 3100 to 15900 relative difference to postulate position The significant raise in maximum in the N_u be present quantified elect 3.0593 and the maximum rise in the (F_f) was 3.11 in contrast with the slick tubing. It was also stated that these correlations predicted the estimates of ?? and Nu with an average absolute variance of 2.1 % and 3.1 % in the context respective of concentrated factors.

Sharad et al. [9] investigated the efficiency of a CFD-based SAH. Simulated ruggedness for, he used an arc-shaped geometry composed of thin circular wire. Arc-shaped geometry's impact on F_f (friction factor), constant of HT, and efficiency improvement be situated evaluated for a set of conditions for friction factor (Re range 6100 - 18100, solar energy from 0.333 to 0.666 to 1000 W/m², alpha/90). To one hand of the surface absorbing material, the ribs (arc-shaped wires) are supplied and the opposite side is held smooth. It was noted that as the Re rises, Nu rises.

Although the friction factor decreases as the Re increases for all $\alpha/90$ and e/D assemblies and The highest value of the overall ratio of change is 1.7 for the e/D -related roughness geometry of 0.0426 and $\alpha/90$ of 0.333 for the set of parameters considered.

Singal et. al. [10]. In the form of a mixture obliged, with ribs, and circumferential sections attached to an A_{bp} , Quantitatively writing, examined the TH_{eff} . of SAHs with a roughness element. The blend of transverse ribs and inclined grooves mounted to the A_{bp} was examined with parameters such as Re scopes from 2000 to 14000, $e = 1.6$ mm, $W/H = 10$, $P/e = 3-8$, $P = 5-13$ mm, $e/Dh = 0.030$ in this study of the friction characteristics and HT concentration. The specificities with HT that roughness or resistance was first measured and then the smoother pipe is comparable to it. It's stated this the geometry with a P/e value of 8 results in maximum thermal efficiency under the same flow conditions. Besides, The maximum value for HT observed designed for the best thermal efficiency was also accounted for.

Bhushan et. al. [11] The correlations of N_u in addition to F_f for SAH with roughness aspect were investigated in the form of protrusions/dimples added to the absorber plate. It was examined those correlations of N_u and F_f be situated generated by the need for data set to anticipate the execution of the framework with such a kind of roughened absorber plate as a system feature then working constraints. Now comparison toward smooth duct for an examined parameter set, the highest increase in N_u and F_f was 3.899 and 2.2345 times were identified for being discretely, and the most extreme increase in the coefficient of HT was found to occur intended.

Samuel [12] To determine the efficiency using a very simple moving plate heating model, examined the solar air heating collector. The efficiency can be approximately 0.5 for the ambient air temperature $t_a = 40$ °C, for the theta value of 50 °C approximately 0.45, and for theta value of 60 °C is about 0.37.

Dhiman et.al. [13] The SAH through a full crib roughness element placed now a novel parallel stream was analytically investigated toward concluding TH_{eff} . For the study of SAH TH_{eff} , a mathematical model was developed and measured using a developed PC code that uses an iterative method of arrangement. It was recorded that with an average blunder of 9.2%, the difference between the results after simulation and exploratory knowledge and the mathematical model generated gives fair expectations of the execution of a SAH as well could be situated as a helpful project instrument designed for upcoming advancement toward mollifying detailed submissions.

Patel et. al. [14] By using B_f and \log_f toward the growth of the warm air enactment, investigated the DPSAH. This investigation learning is a close investigation of the B_f and \log_f embedded classified the DPSAS's drain with metal sinewy strings. In comparison to the SAH with B_f and \log_f , the maximum sun-based radiation was recorded In the membrane of metal sinewy wires

style DPSAH and the highest efficiency was picked up in the DPSAH evaluated to another, with the metal sinewy membrane.

Chamoli et. al. [15] Using arbitrarily corrugated on both sides by the A_{bp} to boost the efficiency, investigated the D PSAH. It integrates the increase in HT, DPSAH design, fall in Pressure, and duct stream phenomenon. The output of the DPSAH and the many techniques that underestimate its performance are discussed both experimentally and analytically, and numerical models of a few DPSAH designs are discussed. It has been reported by there is enormous scope for future research on the top and bottom parts, DPSAH coordinated by the roughness factor going on the A_{bp} surface. If the depths of the duct and volume of air circulation Rate are identical to the top and bottom vents on each, the most extreme efficiency is obtained.

Patel et. al. [16]. Towards growth the TH_{eff} , investigated the DPSAH using fins, baffles, then permeable media also calculated the effect of different types of media on the efficiency of DPSAH's. The effects of significant air velocity, temperature differential, mass flow rate, midair pressure differential parameters were observed for these performances to be contemplated. The highest efficiency was stated to be observed when the absorber material was still in the solar uncoated metallic wiry sponge. It was less cost-effective, and market access was easy.

Kumar [17] tested the effectiveness of the DPSAH through artificial roughness using CFD. This circular wire, nV_{rib} , also nV_{rib} through openings were V-shaped unevenness geometries used. Roughness parameters are 6 as relative roughness width (W/w), comparative breadth (g/e) is 1.0, comparative length (Gd/Lv) is 0.699, aspect ratio (W/H) is 12, relative roughness height (e/D) is 0.0433, comparative ruggedness pitch (P/e) is 10, and attack the degree is 60° . The rise in HT has been stated to have been extended to 1.7 times with the heat transfer of the seamless surface for nV_{rib} , increased to 4.7 times for multi V-shaped, and 5.6 times for nV_{rib} by space of ribs.

Promvong et. al. [18] For the thermal output of turbulent channel flows over the absorber plate having differently designed ribs, investigated the SAH. The key objective of this analysis was to enhance the experimental results information on different rib shapes with a comparable e/H ratio of 0.3 imposed on a duct with turbulent duct flows with a high aspect ratio of 4000 to 16000. Instead of the rectangular one, the staggered triangular rib should be connected to achieve risen HT and TH_{eff} . of near 57.5 %, moving towards to the shorter exchangers and the absolute best control at the lowest Re numbers for all ribs.

Saini et. al. [19] experimentally investigated the SAH because of the friction factor of the arrow wire for the development of Nu to increase the rate of HT, Nu comparisons. Aimed at this investigation, A movement for air in the conduit was taken in parallel. It was stated that the most extreme increase in Nu keeps on measured as 3.808 often the angle of absolute curve comparison

circumstances (α) = 0.3333 during this peak of friction factor = 0.0422, the friction factor increase was 1.75 times compared to these parameters only.

Chander et. al. [20] To analyze the friction factor, HT, and thermo- hydraulic efficiency properties of the stream in a rectangular duct, investigated the SAH with nV_{rib} together to this side, with the dispersed V_{rib} connected of the A_{bp} as a roughness feature. The rectangular duct with Re scope from 4000 to 12000, aspect proportion of 12, V_{rib} depth to a radius of the hydraulic proportion beginning 0.0266 to 0.0577, V_{rib} through drop to peak proportion scope average 9, angle of attack (α) scope from 40° to 80° , spaced dimensions of V_{rib} to the ratio of V_{rib} peak = 4.5, the width of distance to an altitude of V_{rib} proportion = 1, relative spaced pitch for V_{rib} = 0.65 and 2 total of gap (n) placed V-leg along both sides were used. The 2 highs for the N_u related to the 6 and 12 and the decline in the N_u were recorded to rise more than 0.044 in the $/ Dh$ and the extreme growth in the N_u then the thermo-hydraulic output was 3.34 and 2.45 separately.

Kant et. al. [21] Examined the DPSAH for different performance enhancement methods. by lowering the misfortunes of the surface of the collector by supplying the best possible isolation and extending the natural convection constant amid the working fluid and the heat collecting surface through growing the HT field, the efficiency of a customary SAH could be adequately enhanced. The double-pass design will boost this heat transfer field. He used components for compact beds, sides for perforated absorption, and extended Layers. The objectives of this article were to analyze different methods of HT increment used in DPSAHs. It has been stated that it is possible to use the recycling principle to grow the TH_{eff} of DPSAHs.

Singh et. al.[22] studied the DPSAH through an assembled bed as a part of roughness to improve thermal efficiency. The material used in this investigation was the porous assembled bed of DPSAH in an upper duct. In contrast to an assembled bed, the thermal efficiency improves dramatically while adding porous medium to the bottom tube, and SAH excluding an assembled bed. In this study, a large literature review of double channel DPSAH was seen to stress the importance of dual-channel assembled bed DPSAH's. The HT constant through assembled bed SAH has been reported to increase substantially and thus improve thermal efficiency. The hypothetical and exploratory reviews were possibly recorded to demonstrate that the dual-pass, for example, counter and parallel flow assembled bed SAH, works superior to the designed single-pass bed SAH due to the decrease in thermodynamic troubles of the double duct system's inside and back surfaces.

Murugavel et. al. [23] experimentally tested the double-pass SAH with thermal energy sourcing. sodium silicate was utilized as a medium for utilization in heat energy on the absorber plate in the aluminum round and hollow (cylindrical) capsules. The experimental research was performed to test the efficiency of the DPSAH under the K.R. metrological environment with different

setups. Nagar, which is in the state of Tamil Nadu, India ($9^{\circ} 11'N$, $77^{\circ} 52'E$). It was stated that the paraffin wax transfers almost high-temperature air for the rest of the day as energy storage material in SAH and the output is also higher in the mid-night hours and the capsules are put on the A_{bp} of DPSAH where the effective one.

Mirzaei et. al.[24] tested the SAH to find the right procedure. Try various items with a single pass and DPSAH collectors Including layers of WM and ordinary and punctured covers rather than an absorber plate by outline and inspection. The porous media has been mounted around the collector this aims to maximize porous structure in a way that and a slight pressure drop. The primary objective of the goal of this work was to tentatively analyze the SAH output and recommend the arrangement that prompts maximum thermal efficiency. To frame the same solar-based collector, the design and investigation of the experimental technique were used and the knowledge was dissected with SPSS-IBM. At an MFR 0.032 kg / s , the most extreme regular proficiency was recorded to be 54.8% . It was received from the DPSAH collector as well as a corrugated layer of a fourth cover, even though at the comparable flow rate, the most extreme means TH_{eff} acquired from the DPSAH of CF from a standard shield case cover was found to be 50.9% .

Nowzaria et. al.[25] Quantitatively examined the DPSAH in which the A_{bp} was exchanged with the opening of 14 thin steel WML and placed parallel to the glass in the channel. To reduce the pressure drop, the separation between any arrangement of WML was 0.50001 cm . The black paint was added to WML until they were put into the collector. The maximum temperature gradient (53° C) was achieved at a gradient of 0.011113 kg / s and the mean output of the DPSAH collector with a channel height of 3 cm was 53.7001% for the MFR value of 0.037001 kg / s .

Shalaby et. al. [26] Evaluated, numerically and practically, the DPFPSAH and the V-shaped corrugated absorber plate DPVCPSAH for TH_{eff} , i.e. F_c . To measure the change in the thermal properties, a mathematical model was carried out. Various measurements and comparisons were performed, such as airstream outlet temperature, plate temperature absorber, double pass finned power at the outlet. DPVCPSAH was reported to be more effective from the 9.3 to 11.9% range compared to DPFPSAH, there was an improvement in thermal efficiencies of DPFPSAH and DPVCPSAH with an improvement in MFR value until it reached 0.044 kg / s , past which the TH_{eff} expansion of both systems was irrelevant, the thermal-hydraulic efficiency of DPVCPSAH has been reported to have reached 0.044 kg / s ,

Aldabbagh et. al. [27] experimentally evaluated the SPSAH and DPSAH with the roughness portion attached as a fin and used a steel wire mesh to find the thermal output on the absorber plate. The impacts on the TH_{eff} and an exit varies of Temperatures between 0.01222 kg / s and 0.03888

kg / s of the MFR of air was studied. The porosity used is made up of an absorbent medium used consists of layers of SWM mounted at a distance of 1 cm above each other in an arrangement from base to top to provide more absorbency then towards decrease the P_d over the SAH. The longitudinal fins were added and settled along the higher and lesser passage for the SAH to increase the C_{SA} . The second point for this research was to investigate the effect on the TH_{eff} of the primary passage height of the SAH. It was recorded that the extreme TH_{eff} obtained was 59.6233 % and 63.7411 % respectively designed for both SPSAH and DPSAH for the constant MFR of air = 0.03801 kg /s.

Amiable and Tiruneh [28] did CFD research which was used to perform simulation analysis of the flat plate natural convection solar air heater. For the analysis under the environmental conditions of Addis Ababa, Ethiopia, a solar air heater with a single glass shield flat plate solar collector with an air gap is chosen. The goal of the analysis is to find optimum angles of inclination considering the natural fluctuations, find optimum air gap width, and describe the effect on the collector performance of the incident radiation magnitude and ambient temperature. The governing continuity, momentum, and energy equations were regarded in multiple dimensions for modeling the system. By adjusting the angle of inclination, it was noticed that for November, the optimum angle of inclination that provides maximal energy gain with better mass flow rate and temperature increase was 450, while for May it was 150. The two-pitch angles reflect the two extreme seasons of the year. A collector with 50 mm channel depth was also found to achieve better output velocity and temperature and maximum energy gain, but comparable to 60 mm and 70 mm depth for a 2 m long collector. The performance of the simulation is comparable to the experimental findings published in the literature, which are already accessible.

Chabane et al. [29] experimentally studied the TH_{eff} of a SPSAH with five attached fins. To improve the heat exchange and make the fluid flow in the channel uniform, longitudinal fins were used inferior to the A_{bp} . The impact of the air MFR on the temperature of the outlet, HT in the thickness of the SAH, and T_{thp} were studied. For two air MFRs of 0.012 and 0.016 kg/s, tests were carried out. In comparison, for the 0.012 and 0.016 kg s⁻¹ with and without fins, the highest performance values achieved were 40.02%, 51.50%, and 34.92%, 43.94%, respectively. A comparison of the effects of SAH MFRs with and without fins reveals a major increase in thermal efficiency.

Alsanoosi and Aboghrara's [30] study outlines the SAH's experimental analysis of outlet temperature and efficiency. The experimental test was planned and produced to research the effect of jet impingement on the corrugated absorber layer through circular jets in the SAH duct flow and compared to traditional solar air heaters on the flat plate absorber. Air and solar

radiation are studied under the control of the MFR on the temperature and quality of the outlet air. The findings show that the impingement of the flow jet on the corrugated platform absorber is a good HT enhancement feature. The current investigation concludes that HT on SAHs is greatly affected by the MFR of air. And almost 14 % better than the smooth duct is found in terms of the thermal performance of the planned design duct. At 500-1000 (W/M²) SI, 308K atmospheric temperature and 0.01-0.03(Kg/s) MFR. If the amount of the MFR increases, the TH_{eff} increases.

Karwa and Sharma [32] provide a comprehensive mathematical model of a once-through solar water heater for efficiency analysis. The model is validated against the effects of experiments. It was used for a variety of architecture, ambient and operating parameters, and HT enhancement on TH_{eff} and pressure drop to research the solar water heater output. Depending on the MFR, the selective coating ($\epsilon = 0.1$) collector has TH_{eff} advantage of 9-16 %. Collector of 2 mm thick, brazed, or 0.5 mm thick fins Laser or ultrasonic welded thick fins has the same performance. Usage of HT enhancement products, such as a twisted film, for three times HT enhancement, will increase the collector's TH_{eff} by 5.3-6.2 %. In the form of concept graphs, the outcomes of the analysis are described along with the effects of differences in different parameters.

Kumar and Chinnapandian [33] studied in both N_c and F_c, the design and creation of an FPC of SAH, and it were observed that the collector efficiency in N_c offered high efficiency compared to the collector with F_c. The thermal loss in the F_c, however, is slightly smaller than the normal convection. Besides, the results showed that in F_c, the average air velocity was around 25 % higher than the N_c which is significant in solar dryers. The collector efficiency of N_c is 18.6 trillion times higher than the collector efficiency of induced convection at mid-time.

Alamar et al. [34] did a CFD simulation of two-phase flow inside a thermosiphon is in this analysis. The results of the fill ratio (ratio of liquid volume to evaporator volume) and the A⁰ on its TH_{eff} in terms of temperature distribution and T_{HR} are studied by heat pipes using FLUENT (ANSYS 15). CFD simulation results were compared with reported experimental evidence indicating strong agreement for temperature distribution and T_{HR} with a maximum variance of 4.2 % and 8.1 %, respectively. Besides, numerical A⁰ results were also compared in terms of T_{HR} with experimental data, giving a maximum deviation of 1.3 %. Using validated CFD modeling, the results revealed that there was a substantial rise in evaporator temperature at a medium fill ratio and a medium A⁰. Concerning the T_{HR}, with all the heat input values used, a fill ratio of 65 % and an A⁰ of 90 % provided the lowest T_{HR}.

Dahmer et al. [35] experimented by using real-time weather data from two cities: Perth, Australia (a representative city in the southern hemisphere) and Amman, Jordan (a representative city in the northern hemisphere), the influence of the solar collector field,

collector slope, hot water temperature and flow rate on system output were investigated. The simulation findings revealed that the two cities had identical SI during the summertime and that at a relatively high COP system, the solar adsorption chiller could effectively provide cooling. The mean COP system was 0.491 for Perth weather conditions and 0.467 for Amman weather conditions for residential cooling with a cumulative CPC (Compound Parabolic Collector) solar collector area of 36.22 m², while the cooling power was 10.3 kW for Perth and 8.46 kW for Amman, respectively, at peak hours and 80 °C hot water temperature, with a 0.33 kg / s hot water flow rate.

Kabul et al. [36] conducted an inclusive experimental model of adapted coaxial heat pipe inserted inside the evacuated glass developed and analyzed. The annulus was charged with two separate refrigerants R-22 and R-134a between two concentric tubes conducted by the heat pipe. The tests were performed at Alexandria in the summer months. At four separate air MFR of 0.0051, 0.0062, 0.007, and 0.009 kg / s, the coaxial heat pipe was checked. The filling ratio and the type of refrigerant have been experimentally studied as parameters influencing the TH_{eff} of the experimental model. The results show that during the experiment time, the overall improvement in TH_{eff} with the changed heat pipe relative to without a heat pipe reached 67 % at $m = 0.009$ kg / s at the optimum tilt angle 2^0 . At the filling ratio of 30 % for MFR $m^0 = 0.0051$ and 0.0062 kg/s and 40 % filling ratio at $m^0 = 0.007$ and 0.009 kg / s, the optimum TH_{eff} was achieved.

Goyal et al. [37] investigated to compare two different types of engineered and manufactured SAH output for N_c and F_c testing. In both convection modes, the SAH with fins is found to be more efficient. FPC for SAHs, one with a fin and the other without a fin. Comparisons were also presented between the measured outlet temperatures of the circulating air, the A_{bp} temperature, and the power output. The SAH with fins is found to be 8.5 % more effective during N_c than the SAH without fins, and the SAH with fins is 10.45 % more efficient during F_c at 280 °C T_a without fins.

Pakdaman et al. [38] deal with an experimental analysis to test various thermal properties of a longitudinal rectangular fins array N_c FPC of SAH. SI and atmospheric temperature have been regarded as separate parameters in the presented scientific model, which may have industrial implications. Compared to other related research, the specific distinction in this analysis is the presentation of an observational model for rectangular-finned SAHs. This model proposes design principles and thumb laws and displays the estimates of the parameters of the design. Based on the order of magnitude study, the key parameter that characterizes the system's thermal activity is SI. Besides, exergy analysis and optimal conditions have been conducted in which the system has the maximum TH_{eff} was measured.

Kumar [39] performed an analysis of the transfer of natural convective heat from the horizontal rectangular SAH that has been experimentally studied. It was observed that air is heated due to the greenhouse effect, resulting in a lower density allowing air to rise and flow. It often allows the process to bring in fresh air and therefore repetition. Many parameters were measured and considered in good alignment with the results obtained from several correlations available in the literature, such as N_u , Rayleigh number, HT rate, and temperature difference.

Karwa and Srivastava [40] examined the effects of a SAH's TH_{eff} study with v-down discrete rib roughness on the A_{bp} 's airflow side, which provides hot air for space heating applications. The air heater runs at a set temperature of 295 K from the conditional space in closed-loop mode with inlet air. The atmospheric temperature ranged from 278 K to 288 K, referring to Western Rajasthan, India's winter season. The findings of the study are displayed in the form of output plots that a planner will use to measure the optimal airflow rate at varying atmospheric temperatures and values for solar insolation.

3.1 Thermal Analysis of Flat Plate Collector

Energy balance of the A_{bp} , under steady-state condition yields:

$$= A_p S - q_L \quad (3.1.1)$$

where q_u = useful heat gain

A_p = area of absorbing plate

S = incident solar flux absorber in collector

q_L = rate at which energy is lost

Heat transfer rate to the working fluid is;

$$= \dot{m} (T_{fo} - T_{fi}) \quad (3.1.2).$$

where, \dot{m} = mass flow rate of fluid, kg/s

C_f = specific heat of fluid J/m²K

T_{fi} = fluid temperature at the input of collector

T_{fo} = fluid temperature at the outlet of the collector

Solar flux incident on the top of the collector is;

$$I_T = I_b r_b + I_d r_d + (I_b + I_d) r_r. \quad (3.1.3)$$

$$r_b = \frac{\delta \sin(\Phi - \beta) + \cos \delta \cos \omega \cos(\Phi - \beta)}{\sin \delta \sin \Phi + \cos \delta \cos \omega \cos \Phi} \dots \dots \dots (3.1.4)$$

$$r_d = (1 + \cos \beta) / 2 \quad (3.1.5)$$

$$r_r = (1 - \cos \beta) / 2 \quad (3.1.6)$$

Where ρ is the reflection coefficient of the ground. The flux S absorbed in the A_{bp} is given as;

$$S = (\tau \alpha) + \{I_d + (I_b + I_d) r_r\} (\tau \alpha)_d \quad (3.1.7)$$

Where, τ = transmissivity of the glass cover system

α = absorptivity of the absorber plate

$(\tau \alpha)_b$ = transmissivity-absorptivity product for beam radiation falling on the collector

$(\tau \alpha)_d$ = transmissivity-absorptivity product for diffuse radiation falling on collector

The instantaneous collection efficiency η_i of a flat plate collector is given by;

$$\eta_i = \frac{\text{useful heat gain}}{\text{solar radiation incident on the collector}}$$
$$= qu/A_c I \quad (3.1.8)$$

FABRICATION OF SOLAR WIRE MESH AIR COLLECTOR

4.1. Experimental Set-Up Fabrication of Solar Wire Mesh Air Collector



Figure 4.1.1: Main body of solar wire mesh air collector

Mainly 5mm wooden plywood is used in the base and the outer wall is fabricated by 10mm wood (meranti wood) and legs are mounted with 2.5inch (63.5mm) wood.

Table 4.1: Wire mesh solar air heater geometric and physical parameters

Length(m)	Width(m)	The angle of collector from horizontal (A^0)	Absorber plate's absorption coefficient (α)	Glass transmittance Coefficient (τ)	Glass absorption Coefficient (α_g)
2	1	45 ⁰	0.95	0.9	0.05



Figure 4.1.2: Installing the thermocouple on absorber plate

In Fig. 4.1 with 50mm (5cm), thermal insulation with an aluminum absorber plate of 22 gauge 0.7 to 0.8 mm (0.027 to 0.032 inch) thick with black paint with sand particles is coated. A thermocouple is installed for measuring A_{bp} temperature.

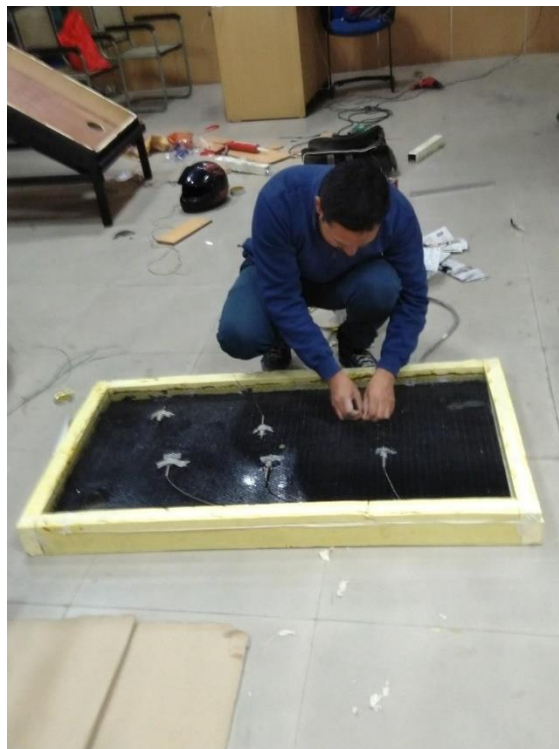


Figure 4.1.3 installing of the thermocouple on wire mesh

In this figure wire mesh is installed in between glass and A_{bp} and wire mesh is placed from absorber plate at a distance of 50mm (5cm). The thermocouple is also installed in wire mesh. and between wire mesh and A_{bp} .



Figure 4.1.4: Fan assembly installation with duct

In Fig.4.1 the duct is installed with a fan. These fans are intended for forced-air cooling of electronic devices with the Ac axial cooling blower exhaust rotary fan. The ac fan aims to protect the electronic devices in the system, as well as any other cooling fan, by holding them at an optimal cooling temperature. By spinning at variable speeds, the fan will produce cool air, thereby defending against thermal variations that will inevitably damage the devices and avoid an early letdown. These apparatuses need to be kept within some particular temperature range to operate efficiently and to prevent overheating, failure, uncertainty, and breakdown leading to a smaller lifecycle. Blowing air along the axis of the fan operates an AC (alternating current) cooling fan. The duct diameter is 90mm.



Figure 4.1.5: Fan back view

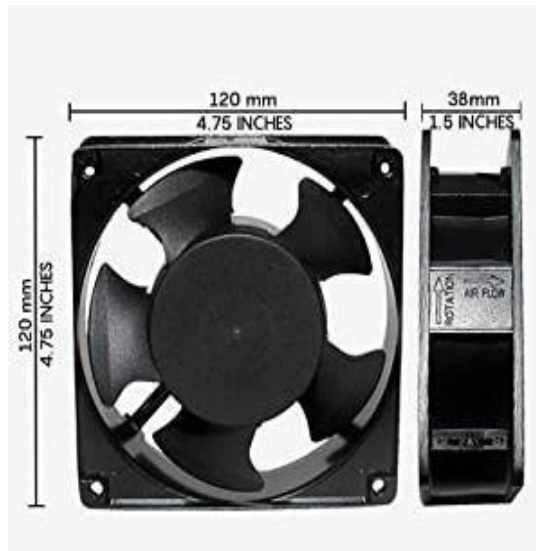


Figure 4.1.6 fan dimensions

Brand	Maa-Ku
Color	Black
Controller type	Button control
Material	Metal
Blade length	110mm
Item dimensions L*W*H	12*12*3.8 cm
Item weight	400gm
Mounting	Flush mounting
Voltage and power	230v & 22 watts

Model no	Ac12038
Rated voltage	220 vac
Frequency	50/60hz
Current	0.14/0.13 amp rated input
Power	22watt
Speed	2600rpm
Size	120*120*38mm
Airflow	90/100cfm

4.1.7 Table technical specification

This exhaust fan is good for small area (5*3*6) feet

This cooling fan is best for cabinet

This ac axial fan is used in multi-purpose functions

This fan is free to stand style

Noise: 40/45 dba, body material: aluminum die-cast with coating fan

Blade plastic p.b.t, bearing type: Sleeve, Color: black



Figure 4.1.7: Installation of fan at the inlet of wire mesh collector

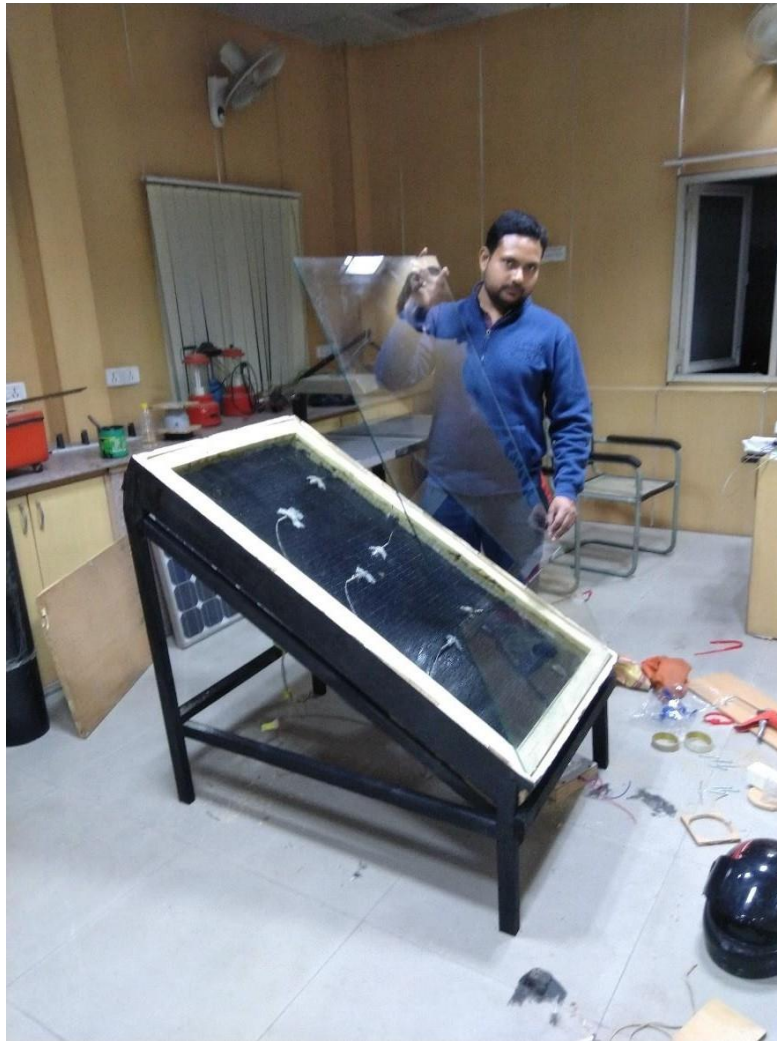


Figure 4.1.8 fixing of glass on wire mesh air heater

Table. Fixing of toughened glass of 5mm thickness

Glass Properties	Toughened glass
Thermal shock Resistance	Up to 250 degrees Celsius
Mechanical Strength	Four to five times stronger than annealed glass
Tensile Strength	65Mpa
Bending strength	120-200n/mm ²
Surface compression	>95mpa
Design stress for architectural purposes	50mpa
Fragmentation	Small round crystals
Conductive for processing	Cannot be cut after toughening

4.2 Instruments

4.2.1 Hygrometer



Figure 4.2.1: Hygrometer

4.2.2 Temperature indicator

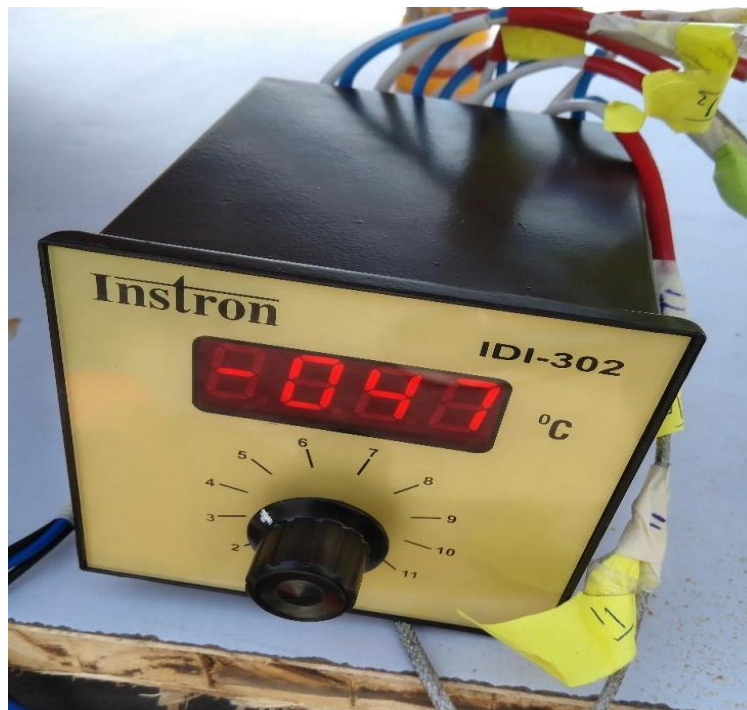


Figure 4.2.2: temperature indicator

4.2.3 Solar power meter

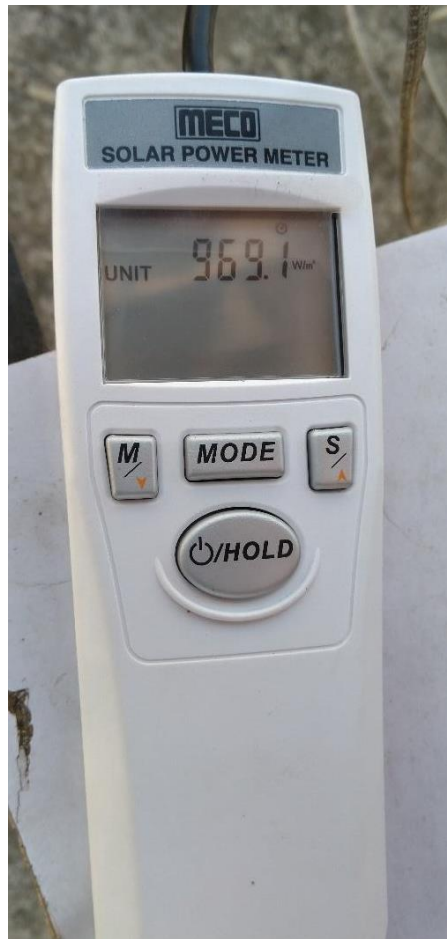


Figure 4.2.3 Solar power meter

4.2.4 Testo 416 anemometer for measuring air velocity



Figure 4.2.4 Anemometers for measuring air velocity

CHAPTER 5

ANSYS 19.2 SIMULATION OF SOLAR WIRE MESH AIR HEATER

5.1. Geometry

5.1.1. Isometric view

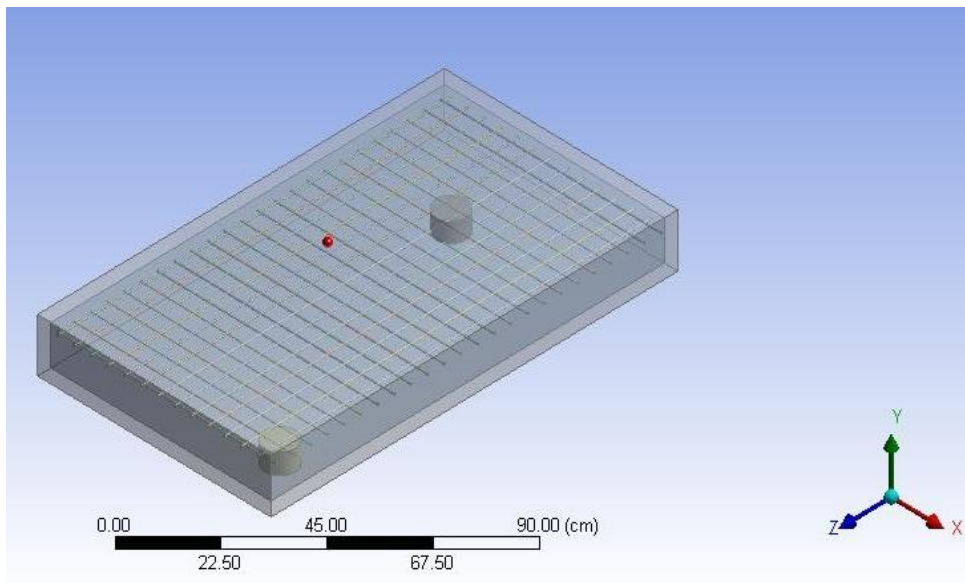


Figure 5.1.1. An isometric view

Top view

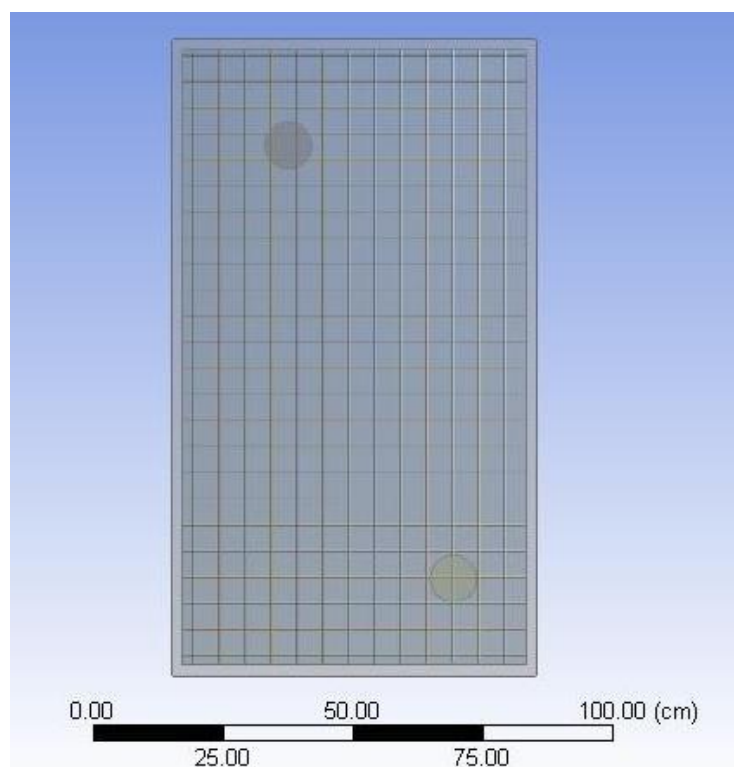


Figure 5.1.1.b Top view

Bottom view

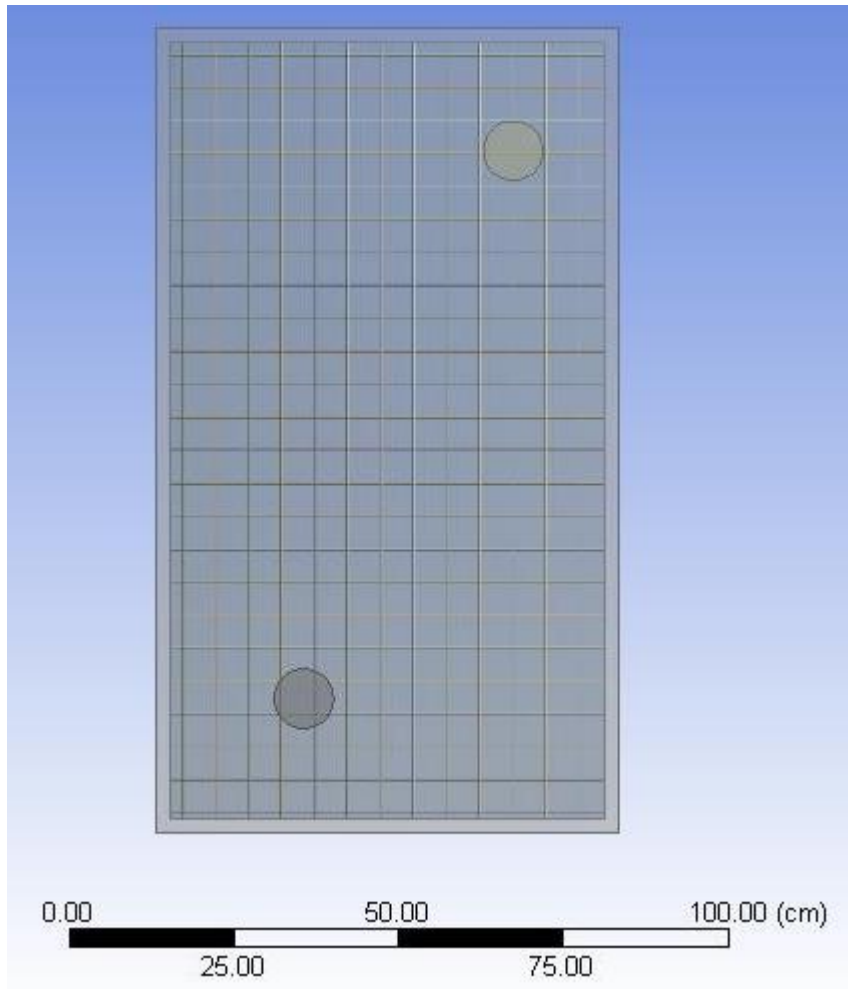


Figure Bottom view

Front view

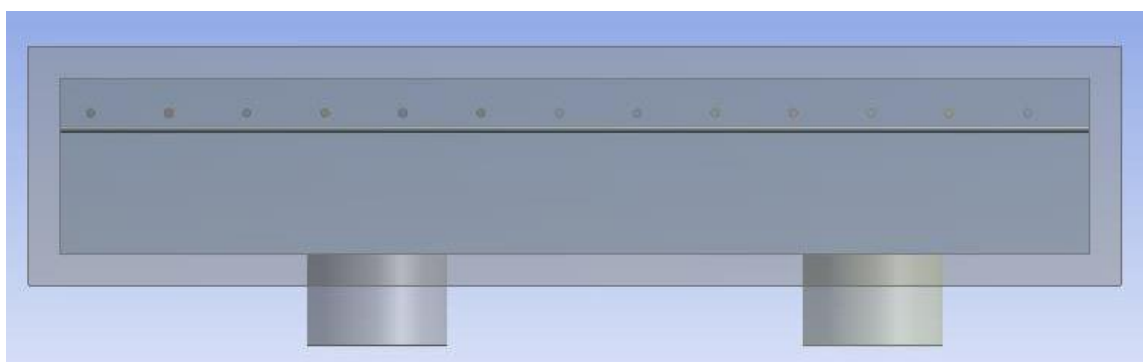


Figure front view

Back view

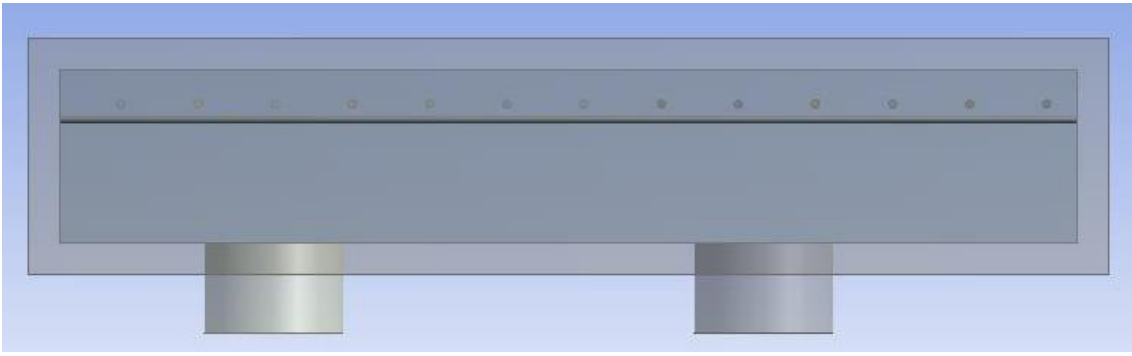


Figure back view

Left view

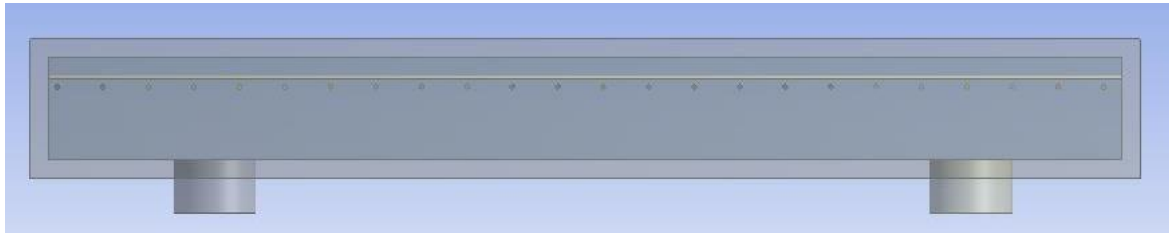


Figure 5.1.1.F left view

Right view

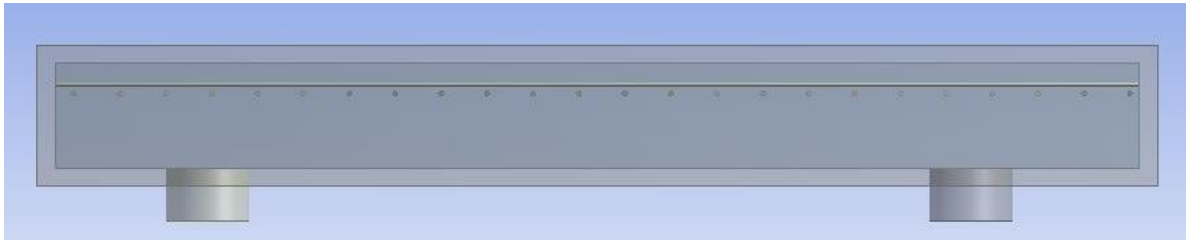


Figure 5.1.1.G right view

CHAPTER 6

RESULTS & DISCUSION

Experimental Results

RESULT

The findings of experimental research on the T_{thp} of a WMSAH are provided in this experiment. In direction to maximize the surface of heat exchange, the temperature of output, and TH_{eff} , a black wire mesh for an A_{bp} must be designed in particular. Tables 6.1a show that for the SAH without wire mesh and a black A_{bp} , increases in MFR affect the temperature of the wire mesh and the temperature of an A_{bp} by 5 to 6 C.

By rates of 5.3 percent and 6.13 percent, the TH_{eff} of the type with WMSAH is shown to be higher than the FPC. We can improve this SI by adding wire mesh above the A_{bp} for moving the HT energy in between the A_{bp} and the wire mesh and the heat energy on an A_{bp} for transportation of fluid with the MFR of 0.012 and 0.016 kg s⁻¹; see Tables 6.3a and 6.3b, and a lesser SI by rates 162 and 187W m², respectively; we can recover this loose SI by adding wire mesh above the A_{bp} for moving the heat energy in between 27.92 percent and 42.83 percent, respectively, were the maximum TH_{eff} figures measured.

Table 6.1a: Temperature variation of FPC and WMSAH along thickness(Y)m

Thickness(Y)m	Flat plate Temperature (°C)	Mesh Temperature (°C)
0	34.8	38.7
0.02	87.5	95.5
0.06	72.02	83.07
1	21.1	31.02

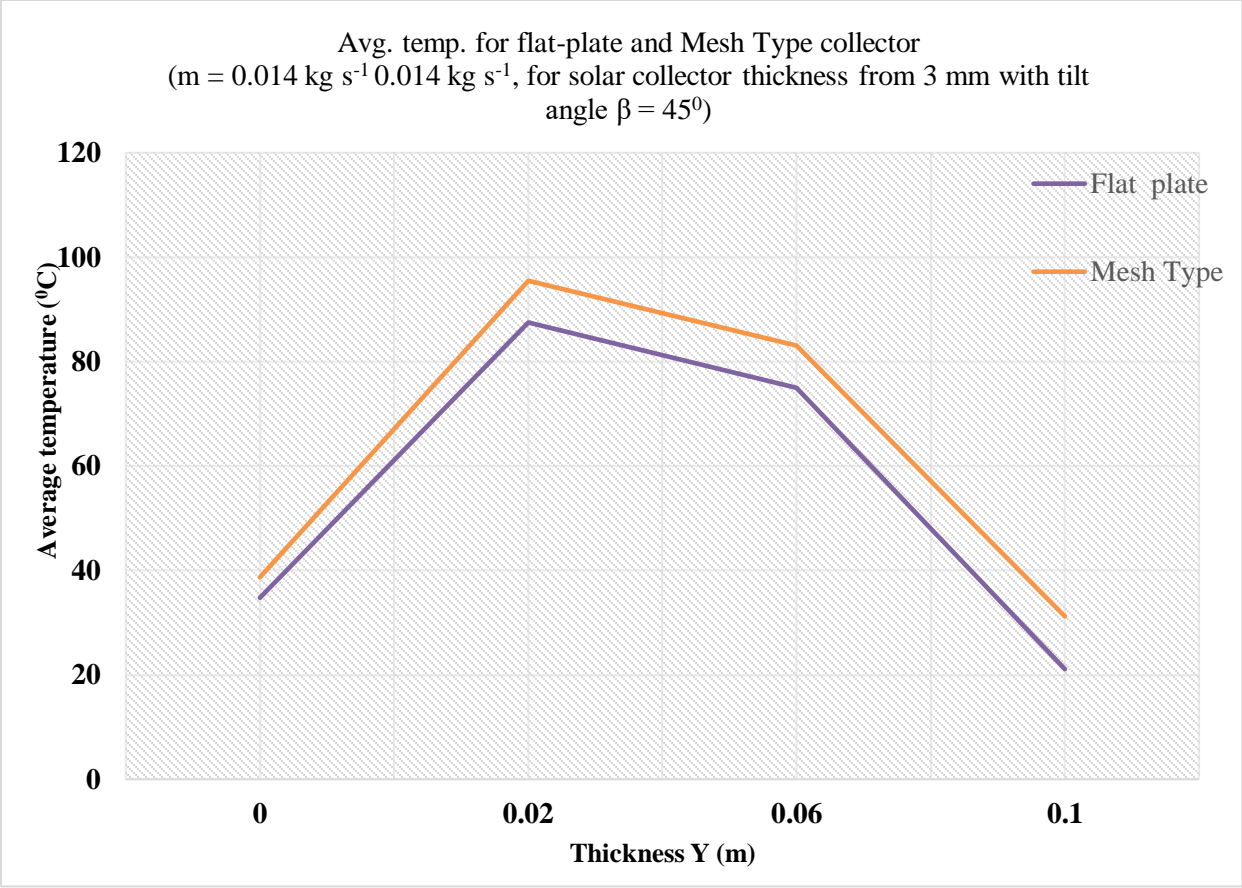


Fig 6.1a: Avg. temp for flate plate and wire mesh type collector ($m=0.014\text{kg s}^{-1}$,for solar collector thickness for 3mm with tilt angle $\beta=45^\circ$)

Table (6.2a) flat plate solar air heater

X(m)	$T_{pl} \text{ } ^\circ\text{C}$	$T_{ab} \text{ } ^\circ\text{C}$	$T_{bp} \text{ } ^\circ\text{C}$	$T_{ep} \text{ } ^\circ\text{C}$
0.388	34.05	87	67.5	28.5
0.776	34.05	88	86	31.65
1.164	35.55	87	79	32.55
1.552	36.2	95	71	30.25

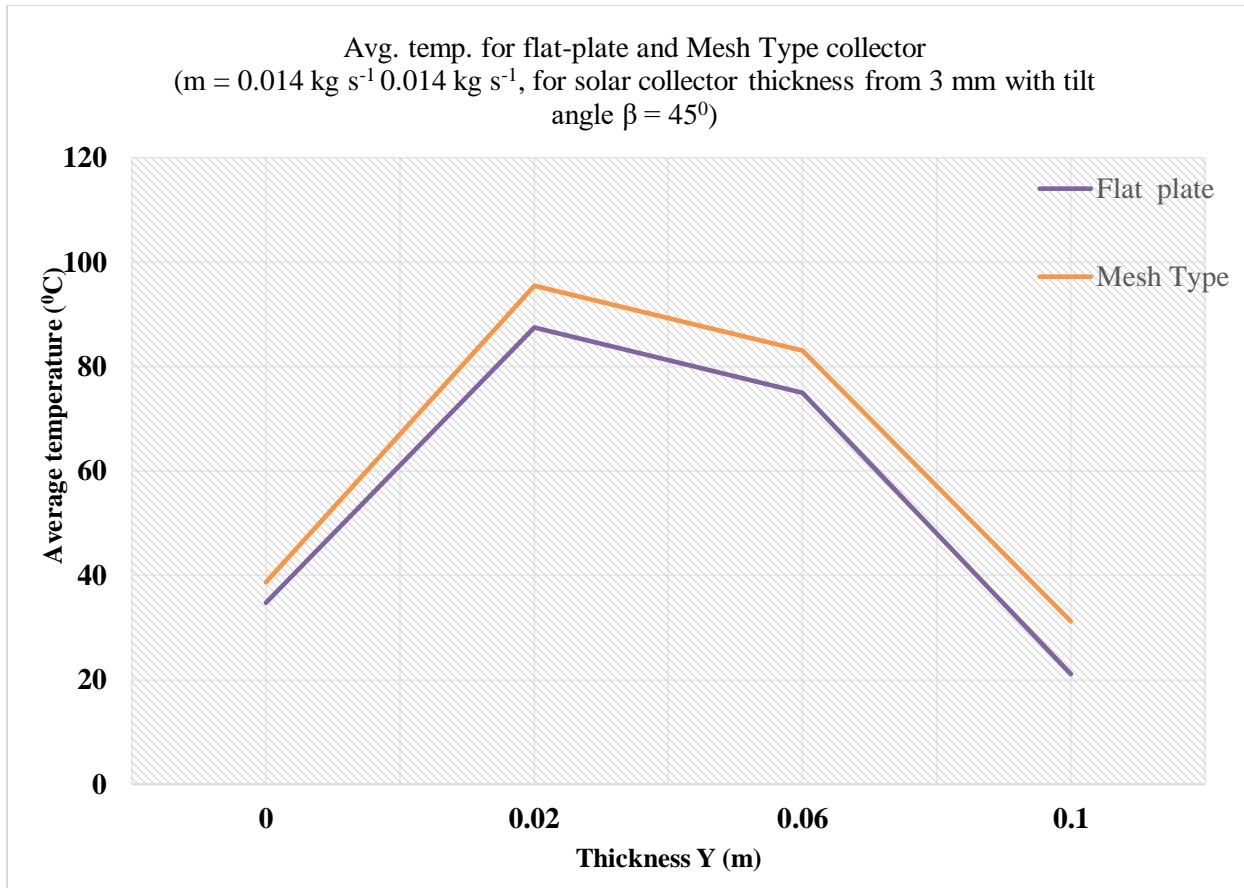


Figure 6.2a: Avg. temp for flat plate and wire mesh type collector ($m=0.014\text{kg s}^{-1}$, for solar collector thickness for 3mm with tilt angle $\beta=45^\circ$)

Table (6.2 b) wire mesh solar air heater

(x) m	T_{pl}	T_{ab}	T_{bp}	T_{ep}
0.388	39.05	95.5	72.7	32.45
0.776	39.35	96.8	91.5	31.5
1.164	41.05	95.4	88.4	30.8
1.552	42.65	101.5	84.3	29.7

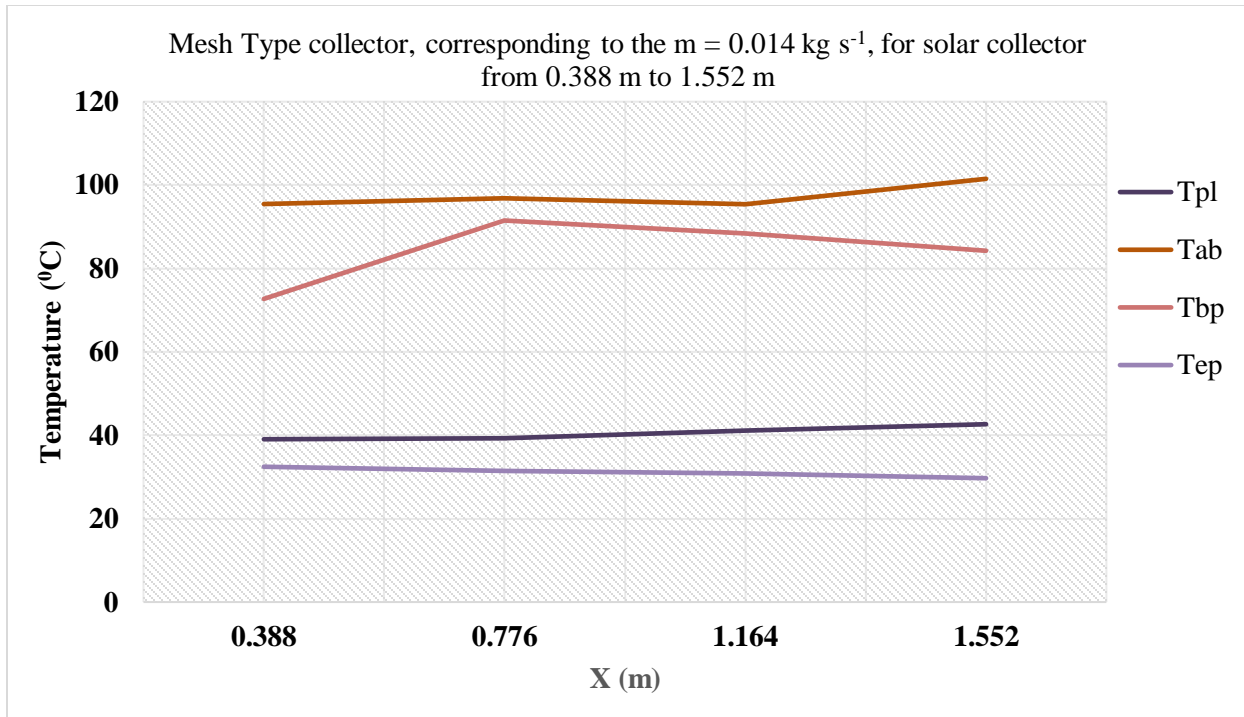


Figure 6.1b: Wire mesh type collector corresponding to $m=0.014\text{kgs}^{-1}$, for solar collector from 0.388m to 1.552m

Table (6.3a) Flat plate type collector SI and efficiency

Time (h)	I (wm^{-2})	η (%)
9:00	421	22.94
10:00	627	29.1
11:00	783	30.02
12:00	867	33.52
13:00	895	34.92
14:00	847	33.59
15:00	725	29.42
16:00	485	27.92

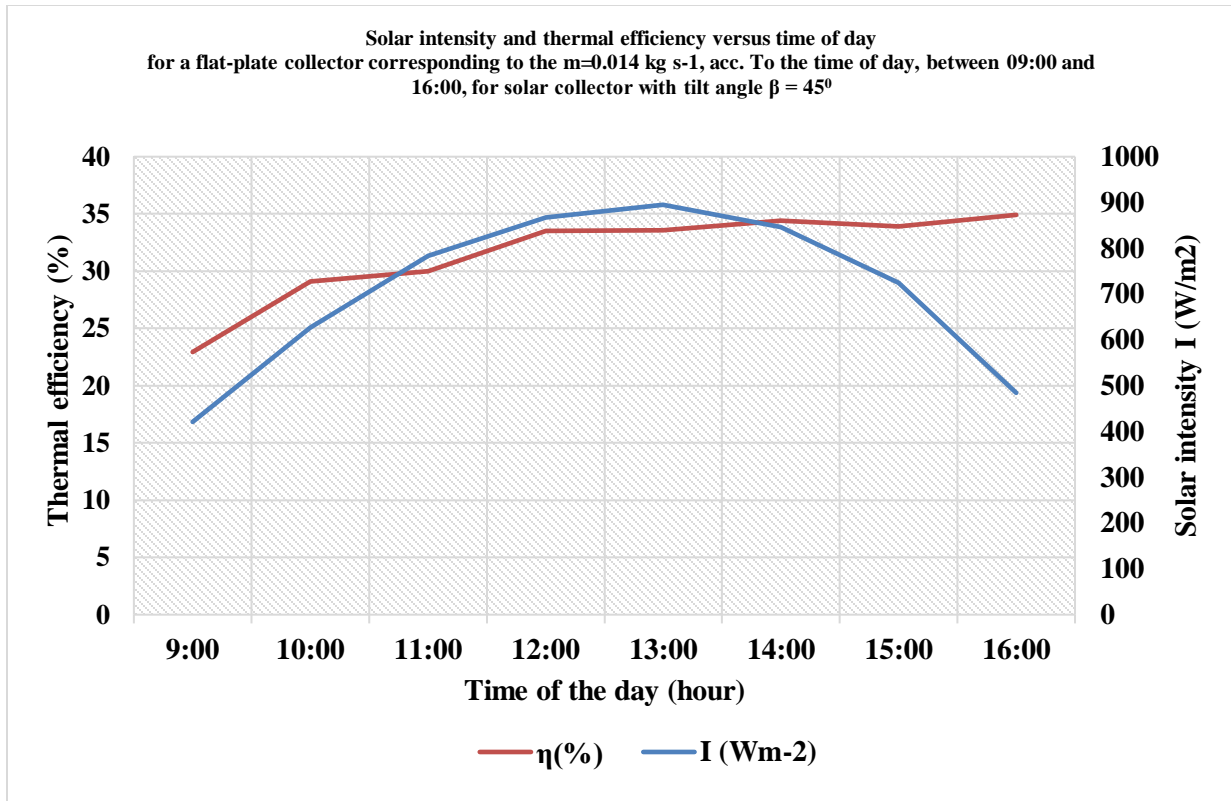


Figure 6.3a: Solar intensity and thermal efficiency versus time of the day for flat plate collector corresponding to the $m=0.014 \text{ kg s}^{-1}$, acc, to the time of the day, between 09:00 and 16:00, for solar collector with tilt angle $\beta=45^\circ$

Table (6.3b) wire mesh type collector si and efficiency

Time(h)	I (wm ⁻²)	η (%)
9:00	521.25	32.67
10:00	712.5	35.299
11:00	843.75	41.525
12:00	925	40.26
13:00	941.25	40.986
14:00	855	44.022
15:00	771.25	43.692
16:00	725	42.834

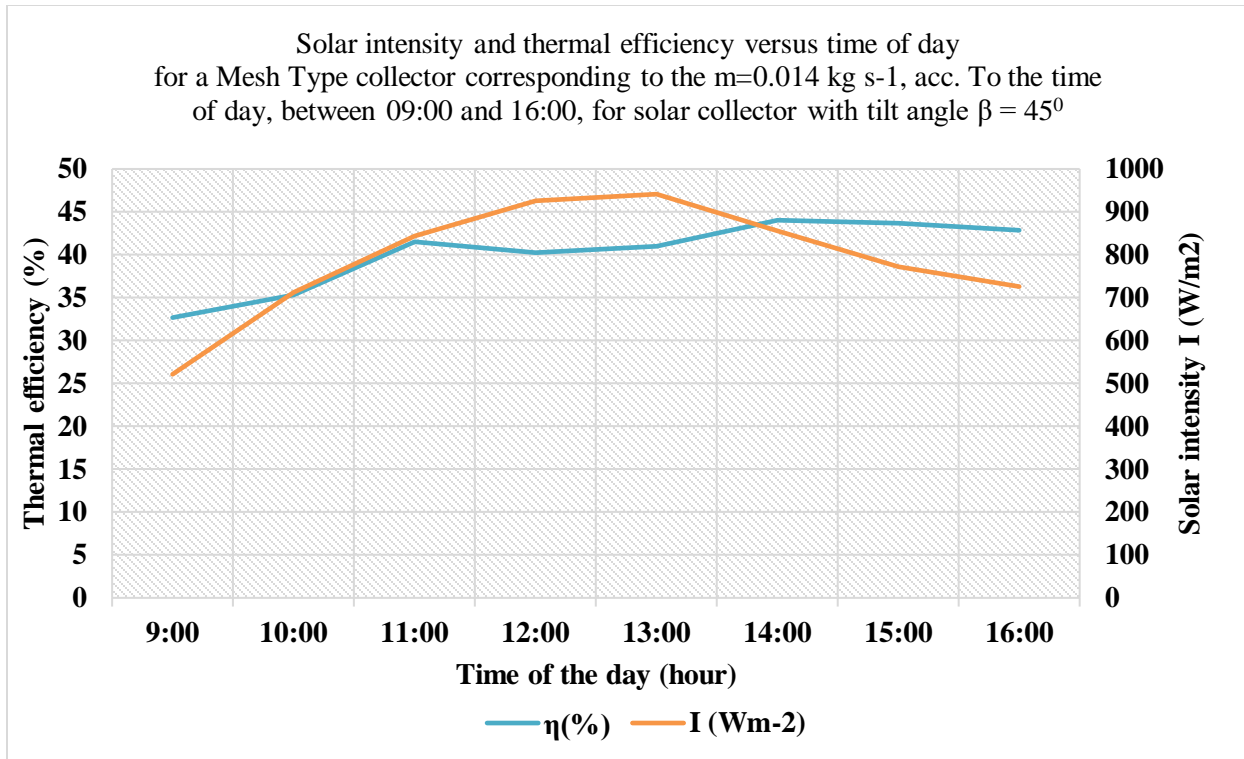


Figure 6.3b'- Solar intensity and thermal efficiency versus time of the day for wire mesh type collector corresponding to the $m=0.014 \text{ kg s}^{-1}$, acc, to the time of the day, between 09:00 and 16:00, for solar collector with tilt angle $\beta=45^\circ$

Table (6.4a) flat plate collector inlet and outlet temperatures

Time (h)	T_{in} ($^\circ\text{C}$)	T_{out} ($^\circ\text{C}$)	T_a ($^\circ\text{C}$)
9:00	29.2	39.1	27
10:00	32.1	49.7	31.4
11:00	34	59.7	32.5
12:00	36	53.5	34.5
13:00	33.5	66.1	32.6
14:00	38.2	65.2	36.5
15:00	38.1	62.7	33.8
16:00	37.5	60.7	32.8

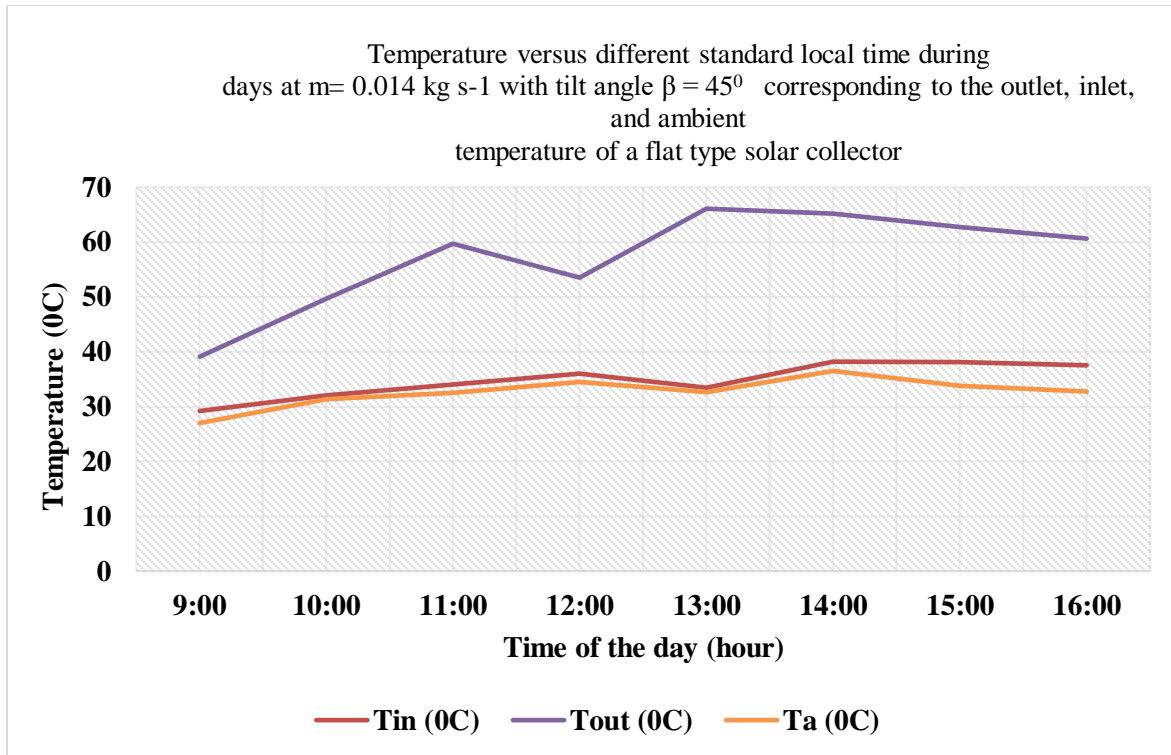


Figure 6.4a: Temperature versus different standard local time during days at $m=0.014\text{kgs}^{-1}$ with tilt angle $\beta=45^\circ$ corresponding to outlet, inlet and ambient temperature of flat type solar collector

Table (6.4b) wire mesh type collector inlet and outlet temperatures

Time (h)	Tin ($^\circ\text{c}$)	Tout($^\circ\text{c}$)	Ta($^\circ\text{c}$)
9:00	30.2	43.1	25
10:00	33.1	53.7	29.4
11:00	35	63.7	30.5
12:00	37	67.5	32.5
13:00	38.5	70.1	30.6
14:00	39.2	69.2	34.5
15:00	39.1	66.7	31.8
16:00	38.5	64.7	30.8

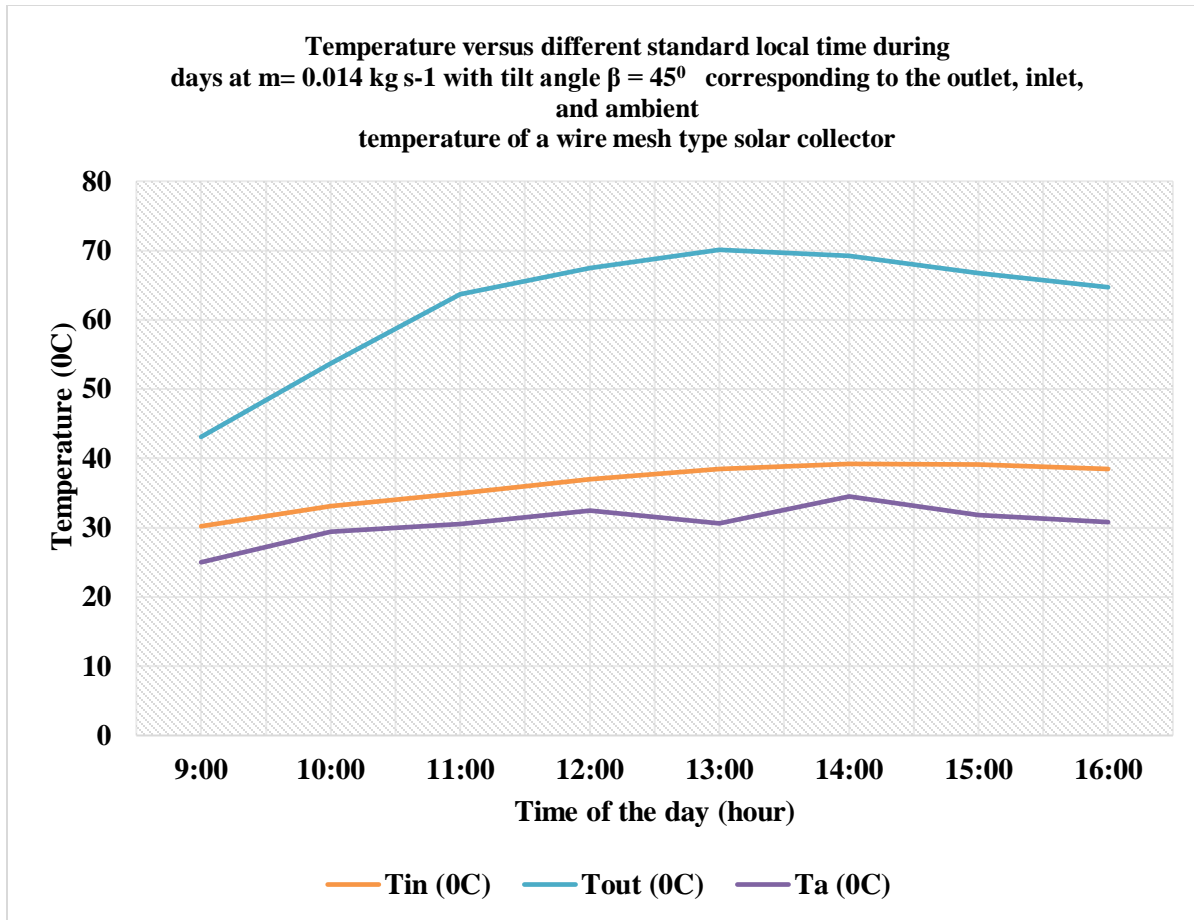


Figure 6.4b: Temperature versus different standard local time during days at $m=0.014\text{kgs}^{-1}$ with tilt angle $\beta=45^\circ$ corresponding to outlet, inlet, and ambient temperature of wire mesh type solar collector

Table (6.5a) comparison between flat plate and wire mesh type collector efficiency

Time(h)	Flat plate Efficiency (%)	Wire mesh collector Efficiency (%)
9:00	22.94	32.67
10:00	29.1	35.299
11:00	30.02	41.525
12:00	33.52	40.26
13:00	34.92	40.986
14:00	33.59	44.022
15:00	29.42	43.692
16:00	27.92	42.834

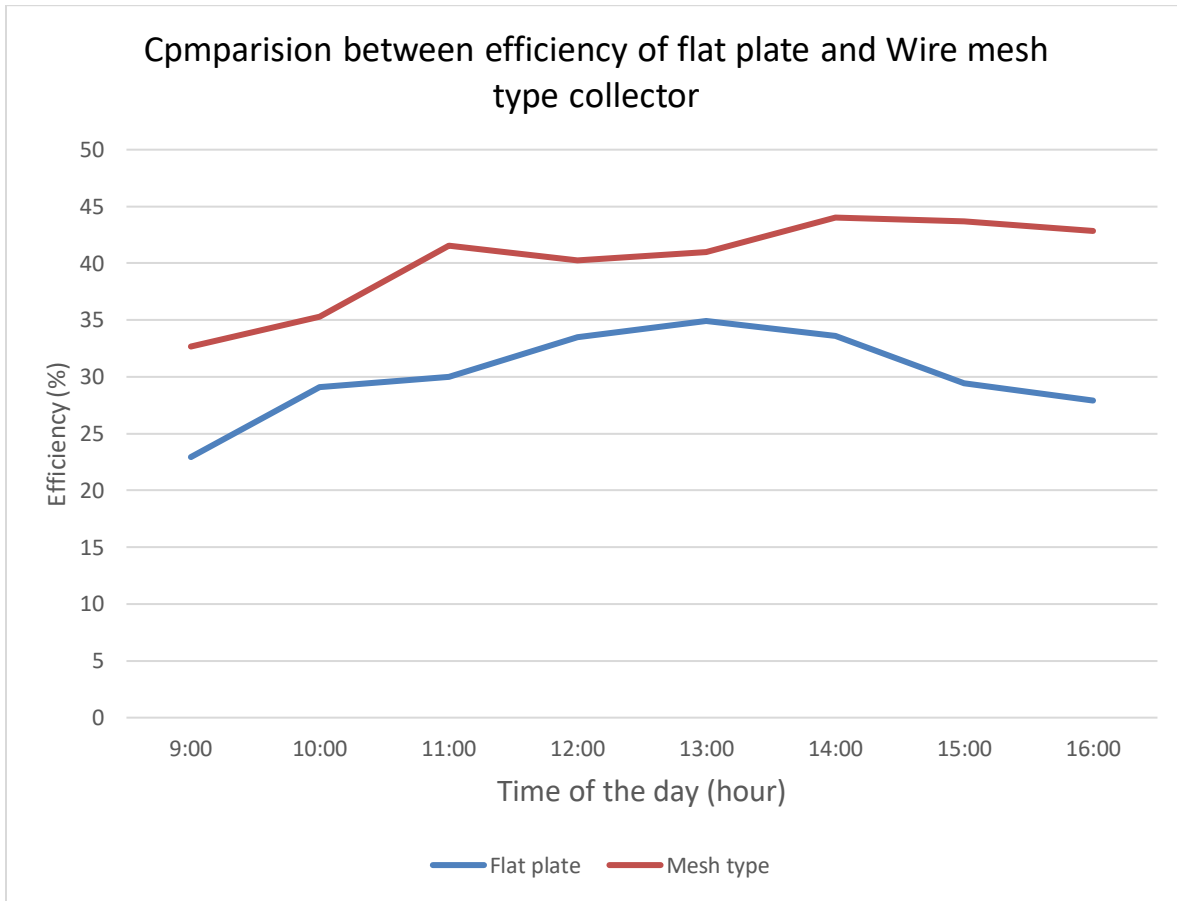


Figure 6.4a: Comparison between efficiency of flat plate and Wire mesh type collector

Discussion

the T_{av}^0C distribution in a SAH thickness and the variation of the T_{av}^0C corresponding to the A_{bp} , wire mesh Figures 6.3a and 6.3b show the difference; at MFR of 0.012 and 0.016 kg s⁻¹, the variation in curves is significant, and the wire mesh's duty is to let convective HT to the A_{bp} and ensure a better heat exchange. Increases in MFR affect the temperature of the wire mesh and the temperature of an A_{bp} by 4 to 6 C for the SAH without wire mesh and with wire mesh, as shown in Tables 6.1a.

(T_{bp} = 75.02 and 83.07 C) and (T_{ab} = 87.50 and 95.5 C) (see Table 6.1a). On a wooden frame, the collectors are mounted. The A_{bp} absorbs the SI that passes through the glass in the field. After then, the heat is transmitted to the collector fluid.

the T_{av}^0C of a SAH without wire mesh for lengths ranging from 0.388 to 1.552 m and MFR of 0.012 and 0.016 kg s⁻¹, respectively. The T_{av}^0C of a wire mesh at a length of $x_2 = 0.776$ m at $m = 0.012$ and 0.016 kg s⁻¹ was ($T_{bp} = 86$), while the T_{av}^0C of an A_{bp} was ($T_{ab} = 91.50$) see Table 6.2a. The WMSAH absorbs more heat from an A_{bp} on average, suggesting that the fluid between the wire mesh and the A_{bp} absorbs heat from the A_{bp} . At point x_2 , the temperature of an A_{bp} is lowered.

In Figs. 6.4a and 6.4b, the difference in T_{av}^0C of both x_1 and x_2 can be seen, indicating that $T_{ab}(x_2)$ ($T_{ab}(x_3)$ and $T_{ab}(x_4)$) $T_{ab}(x_1)$; this shows that the fluid absorbs less HT energy for each point along the length of a SAH except point x_2 . The T_{av}^0C of an A_{bp} decreases slightly as the MFR increases, except in x_2 ; the T_{av}^0C of the WMSAH approaching the T_{av}^0C of an A_{bp} is not approaching, because the fluid takes more HT energy from the A_{bp} and the wire mesh also takes this energy.

6.2a and 6.2b illustrate the T_{av}^0C of a SAH as a function of length, from 0.388 to 1.552 m, for modes with wire mesh at MFR of 0.012 and 0.016 kg s⁻¹, respectively. As can be observed, the curves evolve in an expectable pattern, and the temperature values of the A_{bp} and WMSAH rise in a predictable pattern: ($T_{ab} = 88$ and 96.8 C) and ($T_{bp} = 86$ and 91.5 C) at $x_2 = 0.776$ m, respectively. The fluid absorbs more heat energy from the A_{bp} and the wire mesh, which can be explained.

The temperature of the WMSAH lowers as the MFR increases, indicating that the operation of delivering the fluid takes more heat off the wire mesh and cools it. It should be noted that the T_{av}^0C $T_{ab}(x_1, m)$ $T_{ab}(x_2, m)$ $T_{ab}(x_3, m)$ $T_{ab}(x_3, m)$ $T_{ab}(x_4, m)$ $T_{ab}(x_4, m)$ $T_{ab}(x_4, m)$ $T_{ab}(x_4, m)$ $T_{ab}(x_4, m)$ $T_{ab}(x_4, m)$ $T_{ab}(x_4, m)$. A wire mesh aids in maintaining the temperature of a fluid, suggesting that it serves as a HT energy storage system for the air.

The reason for the difference between Figures 6.4a' and 6.4b' and Figures 6.3a' and 6.3b' is that the wire mesh and A_{bp} were added to the SAH for the best T_{thp} of the SAH; the air is distributed very well and absorbs more HT energy from the wire mesh and the A_{bp} . Because wire mesh obtains more heat due to an increase in heating time through circulating the air inside, and a glass helps to reduce N_c heat losses, the temperature values vary (rise). This exchange occurs along the full length of the collector when wire mesh is present.

The TH_{eff} and SI vary with air MFR, as shown in Figures 6.4a', and 6.4b', 6.3a' and 6.3b'. The TH_{eff} used to evaluate the effectiveness of the SAH is computed; based on both values, the TH_{eff}

improves as the SI and MFR increase over time. WMSAH have higher efficiency than non-wire mesh SAH. The TH_{eff} of a SAH with and without wire mesh is compared in Figs. 6.5a' for two distinct MFR. Tables 6.5a, 6.3a and 6.3b contain the data for each SAH.

At an air MFR of 0.016 kg s⁻¹ and a 45 tilt angle at 16:00 h, the mean maximum TH_{eff} (g= 40.02 percent) was attained by type with wire mesh at SI I= 480 W m². The lowest mean TH_{eff} (g= 34.92 percent) was obtained with type without wire mesh at an air MFR of 0.012 kg s⁻¹ and a 45 tilt angle at SI I =485 W m² at 16:00 h. Based on the performance curves at a tilt angle of 45 [34], the performance curves of two modes of the SAHs evaluated for this work are illustrated in Figs. 6.3a', and 6.3b',6.5a'.

The SAH with wire mesh had a better TH_{eff} than the one without wire mesh, which corresponded to two air flow rates. The flat-plate SAH showed a greater SI than the wire mesh type, depending on air MFR of 0.012 and 0.016 kg s⁻¹. It can be seen that the A_{bp} with the lowest SI has the maximum TH_{eff} , which helps to add wire mesh back to the A_{bp} . Because the air had more time to warm up inside the collector, the SAH heated the air significantly more efficiently at the reduced air MFR.

The change of ambient T_{out} °C and T_{in} °C as a function of air MFR and time during the day is shown in Figures 6.4a' and 6.4b' (please refer to Tables6.4a and 6.4b). The temperature was determined experimentally, and the curves of output temperature tend to increase when the air MFR decreases, as shown in Figs. 6.4a'and 6.4b',6.5a'. The T_{out} °C and T_{in} °C rise with increasing sun SI for a particular air MFR at a constant T_a . The wire mesh has returned to an A_{bp} , which aids in raising the T_{out} °C of air.

For MFR of m=0.012 and 0.016 kg s⁻¹, the T_{in} °C was shown to rise exponentially from morning to evening. T_{in} = 29.2 and 30.2 degrees Celsius at 9:00 a.m., respectively, for ambient temps T_a = 27 and 28.3 degrees Celsius. Due to improved HT to the air flow, the SAHs TH_{eff} improves as air MFR increase, and the temperature differential reduces at a constant tilt angle of 45 degrees. As expected, SI peaks around 13:30 p.m. As the day progresses, the SI gradually lowers.

The modification in air T_{in} °C and T_{out} °C, as well as instantaneous SI levels, are shown in Figs. 6.4a' and 6.4b'. The temperature ranged from 30.6 degrees Celsius. The T_a was used to compare the T_{in} °C's of the two types of SAHs. When determining the performance of the SAHs, the

temperature disparities between the $T_{in}^{\circ C}$ and $T_{out}^{\circ C}$ can be readily compared. The greatest SI is 867 and 895W m² for an FPC and 925wm⁻² and 941.25wm⁻² for a WMSAH. For all of the days in which trials were conducted, it increased in the morning to a peak value and then began to fall in the afternoon, as expected.

CHAPTER 7

CONCLUSIONS

The aim of this research is to look into WMSAH designs and determine their TH_{eff} . In this experiment, a SAH with and without wire mesh attached to the A_{bp} was compared. SI, MFR, SAH surface geometry, and the use of wire mesh back the A_{bp} all affect the effectiveness of SAHs. Due to improved heat transfer to the airflow, the TH_{eff} of the SAH rises as sun SI increases at MFR of 0.012 and 0.016 kg s⁻¹.

The WMSAH has been shown to be more efficient. The WMSAH with a tilt angle of 45 attained the best collector TH_{eff} and air temperature rise, whereas the collector without wire mesh achieved the lowest values. To maximize the effectiveness of the SAH, optimal air MFR are advised. Changes in flow state from laminar to turbulent can be linked to the large increase in efficiency from 0.012 to 0.016 kg s⁻¹. With increasing MFR, the slope of the efficiency curves drops, suggesting a decrease in the loss coefficient. When the T_{in} is close to the T_a , the experimental findings indicate better agreement.

The SI and SAH surface geometry have a big impact on the efficiency of WMSAH. As the MFR rises from 0.012 to 0.016 kg s⁻¹, the TH_{eff} rises as well. SAH have been shown to have better efficiency. The WMSAH with a 45-degree angle produced the best collector TH_{eff} and air temperature rise, whereas the SAH without wire mesh produced the lowest results. At MFR of 0.012 and 0.016 kg s⁻¹, TH_{eff} ranged from 27.92 percent to 42.83 percent, respectively, with and without wire mesh.

REFERENCES

1. Bagga, G. S. (2016). Analysis of Flat Plate Solar Air Collector in Different Convection Mode with Induced Turbulence. *Int. J. Eng. Res. Technol*, 5(7),488- 494.
2. Amibe, D. A., & Tiruneh, A. (2016). CFD Analysis of Heat Transfer and Fluid Flow in Flat Plate Natural Convection Solar Air Heater.
3. Chabane, F., Moumimi, N., & Benramache, S. (2014). Experimental study of heat transfer and thermal performance with longitudinal fins of the solar air heater. *Journal of advanced research*, 5(2), 183-192.
4. Aboghrara, A. M., Baharudin, B. T. H. T., Alghoul, M. A., Adam, N. M., Hairuddin, A., & Hasan, H. A. (2017). Performance analysis of solar air heater with jet impingement on corrugated absorber plate. *Case studies in thermal engineering*, 10, 111-120.
5. A. Saxena, N. Agarwal, and G. Srivastava, "Design and performance of a solar air heater with long term heat storage," *Int. J. Heat Mass Transf.*, vol. 60, no. 1, pp. 8–16, 2013.
6. S. Singh, S. Chander, and J. S. Saini, "Heat transfer and friction factor correlations of solar air heater ducts artificially roughened with discrete V-down ribs," *Energy*, vol. 36, no. 8, pp. 5053–5064, 2011
7. S. Kumar and R. P. Saini, "CFD based performance analysis of a solar air heater duct provided with artificial roughness," *Renew. Energy*, vol. 34, no. 5, pp. 1285–1291, 2009
8. Varun, R. P. Saini, and S. K. Singal, "Investigation of thermal performance of solar air heater having roughness elements as a combination of inclined and transverse ribs on the absorber plate," *Renew. Energy*, vol. 33, no. 6, pp. 1398–1405, 2008.
9. Brij Bhushan, Ranjit Singh, Nusselt number and friction factor correlations for solar air heater duct having artificially roughened absorber plate, *Solar energy* 85(2011) 1109- 1118.
10. M. Samuel, "Efficiency of solar plate air heaters," *Appl. Sol. Energy*, vol. 44, no. 4, pp. 258–261, 2008.
11. P. Dhiman, N. S. Thakur, A. Kumar, and S. Singh, "An analytical model to predict the thermal performance of a novel parallel flow packed bed solar air heater," *Appl. Energy*, vol. 88, no. 6, pp. 2157–2167, 2011.
12. K. Patel, S. Soni, and S. Trivedi, "Comparative Study of Double Pass Solar Air Heater with

- Solar Air Heater with Baffles & With Longitudinal Fins,” pp. 2790– 2794.
13. S. Chamoli, R. Chauhan, N. S. Thakur, and J. S. Saini, “A review of the performance of double pass solar air heater,” *Renewable and Sustainable Energy Reviews*, vol.16, no. 1. pp. 481–492, 2012
 14. K. Patel, S. Soni, and U. Soni, “A Review to Enhance the Efficiency of Double Pass Solar Air Heater,” no. February, pp. 712–715, 2015.
 15. A. Kumar, “Analysis of heat transfer and fluid flow in differently shaped roughness elements on the absorber plate solar air heater duct,” *Energy Procedia*, vol. 57, pp.2102– 2111, 2014.
 16. Pongjet Promvong, Chinaruk Thianpong, “Thermal Performance Assessment of Turbulent Channel Flows over Different Shaped Ribs, ” *International Communications in Heat and Mass Transfer* 35 (2008) 1327 - 1334.
 17. A. Kumar, R. P. Saini, and J. S. Saini, “Development of correlations for Nusselt number and friction factor for solar air heater with roughened duct having multi v-shaped with gap rib as artificial roughness,” *Renew. Energy*, vol. 58, no. 12, pp.151–163, 2013.
 18. N. S. Deo, S. Chander, and J. S. Saini, “Performance analysis of solar air heater duct roughened with multigap V-down ribs combined with staggered ribs,” *Renew. Energy*, vol. 91, pp. 484–500, 2016.
 19. R. K. Ravi and R. P. Saini, “A review on different techniques used for performance enhancement of double pass solar air heaters,” *Renew. Sustain. Energy Rev.*, vol.56, pp. 941–952, 2016.
 20. S. Singh and P. Dhiman, “Thermal performance of double pass packed bed solar air heaters - A comprehensive review,” *Renew. Sustain. Energy Rev.*, vol. 53, pp. 1010–1031, 2016.
 21. S. S. Krishnananth and K. Kalidasa Murugavel, “Experimental study on double pass solar air heater with thermal energy storage,” *J. King Saud Univ. - Eng. Sci.*, vol. 25, no. 2, pp. 135–140, 2012.
 22. Raheleh Nowzari, Nima Mirzaie, L.B.Y. Aldabbagh “Finding the best configuration for a solar air heater” *Energy Conversion and Management* 100 (2015) 131–137.
 23. R. Nowzari, L. B. Y. Aldabbagh, and N. Mirzaei, “Experimental Study on Double Pass Solar Air Heater With Mesh Layers As Absorber Plate,” *Int. J. Electron. Mech.MECHATRONICS Eng.*, vol. 3 Num 4, pp. 673–68.
 24. A. A. El-Sebaei, S. Aboul-Enein, M. R. I. Ramadan, S. M. Shalaby, and B. M. Moharram,

- “Thermal performance investigation of double pass-finned plate solar air heater,” *Appl. Energy*, vol. 88, no. 5, pp. 1727–1739, 2011.
25. A. P. Omojaro and L. B. Y. Aldabbagh, “Experimental performance of single and double pass solar air heater with fins and steel wire mesh as the absorber,” *Appl. Energy*, vol. 87, no. 12, pp. 3759–3765, 2010.
 26. Bagga, G. S. (2016). Analysis of Flat Plate Solar Air Collector in Different Convection Mode with Induced Turbulence. *Int. J. Eng. Res. Technol*, 5(7), 488-494.
 27. Amibe, D. A., & Tiruneh, A. (2016). CFD Analysis of Heat Transfer and Fluid Flow in Flat Plate Natural Convection Solar Air Heater.
 28. Chabane, F., Moummi, N., & Benramache, S. (2014). Experimental study of heat transfer and thermal performance with longitudinal fins of the solar air heater. *Journal of advanced research*, 5(2), 183-192.
 29. Aboghrara, A. M., Baharudin, B. T. H. T., Alghoul, M. A., Adam, N. M., Hairuddin, A. A., & Hasan, H. A. (2017). Performance analysis of solar air heater with jet impingement on corrugated absorber plate. *Case studies in thermal engineering*, 10, 111-120.
 30. KUMAR, S. B. S., & CHINNAPANDIAN, M. The Performance Study Of A Solar Flat Plate Type Air Collector With Natural And Forced Convection. *Journal of Industrial Pollution Control*, 33(2), 1155-1162.
 31. Alammar, A. A., Al-Dadah, R. K., & Mahmoud, S. M. (2016). Numerical investigation of the effect of fill ratio and inclination angle on a thermosiphon heat pipe thermal performance. *Applied Thermal Engineering*, 108, 1055-1065.
 32. Alahmer, A., Wang, X., Al-Rbaihat, R., Alam, K. A., & Saha, B. B. (2016). Performance evaluation of a solar adsorption chiller under different climatic conditions. *Applied Energy*, 175, 293-304.
 33. Kabeel, A. E., Dawood, M. M. K., & Shehata, A. I. (2017). Augmentation of thermal efficiency of the glass evacuated solar tube collector with coaxial heat pipe with different refrigerants and filling ratio. *Energy Conversion and Management*, 138, 286-298.
 34. Goyal, K., Tiwari, S., Prajapati, K., Singh, Y., & Sharma, M. Experimental Performance Analysis of Solar Air Heaters with and Without Fin. *Energy Technology & Ecological Concerns: A Contemporary Approach*, 158.
 35. Pakdaman, M. F., Lashkari, A., Tabrizi, H. B., & Hosseini, R. (2011). Performance evaluation

of a natural-convection solar air-heater with a rectangular-finned absorber plate. *Energy conversion and management*, 52(2), 1215-1225.

36. Karwa, R., & Srivastava, V. (2013). Thermal performance of solar air heater having absorber plate with v-down discrete rib roughness for space-heating applications. *Journal of Renewable Energy*, 2013.